

# ACCEPTED VERSION

Xianwen Hu, Ching-Tai Ng, Andrei Kotousov

## **Numerical and experimental investigations on mode conversion of guided waves in partially immersed plates**

Measurement, 2022; 190:110750-1-110750-16

© 2022 Elsevier Ltd. All rights reserved.

This manuscript version is made available under the CC-BY-NC-ND 4.0 license

<http://creativecommons.org/licenses/by-nc-nd/4.0/>

Final publication at: <http://dx.doi.org/10.1016/j.measurement.2022.110750>

### **PERMISSIONS**

<https://www.elsevier.com/about/policies/sharing>

Accepted Manuscript

Authors can share their [accepted manuscript](#):

24 Month Embargo

#### **After the embargo period**

- via non-commercial hosting platforms such as their institutional repository
- via commercial sites with which Elsevier has an agreement

In all cases [accepted manuscripts](#) should:

- link to the formal publication via its DOI
- bear a CC-BY-NC-ND license – this is easy to do
- if aggregated with other manuscripts, for example in a repository or other site, be shared in alignment with our [hosting policy](#)
- not be added to or enhanced in any way to appear more like, or to substitute for, the published journal article

**28 March 2024**

<http://hdl.handle.net/2440/134615>

**Journal article:**

Xianwen Hu, Ching Tai Ng, Andrei Kotousov. (2022). Numerical and experimental investigations on mode conversion of guided waves in partially immersed plates. *Measurement*, 190:110750.

# Numerical and Experimental Investigations on Mode Conversion of Guided Waves in Partially Immersed Plates

Xianwen Hu<sup>a</sup>, Ching-Tai Ng<sup>a,\*</sup>, Andrei Kotousov<sup>b</sup>

<sup>a</sup> School of Civil, Environmental & Mining Engineering, The University of Adelaide, SA 5005, Australia

<sup>b</sup> School of Mechanical Engineering, The University of Adelaide, SA 5005, Australia

## Abstract

This paper numerically and experimentally investigates guided wave propagation in a steel plate with one side partly exposed to water. The fundamental anti-symmetric Lamb wave ( $A_0$ ) is excited on the dry plate section and travels to the water-immersed plate section, where the generated  $A_0$  wave is mode converted to quasi-Scholte (QS) wave. The results demonstrate that the energy of QS wave converted by  $A_0$  wave decreases when the excitation frequency increases. In addition, it is revealed that the guided wave energy can shift in the frequency domain if the phase velocity of the incident  $A_0$  wave is larger than the sound speed of water. The frequency shift phenomenon should be noticed in practical applications because the behaviors of guided waves vary with frequency. Finally, discussions are provided on the frequency selection for exciting guided waves to detect damage on partially immersed structures and assess liquid properties.

**Keywords:** Quasi-Scholte waves; Lamb waves; leaky guided waves; mode conversion; submerged structures.

## 1. Introduction

Ultrasonic guided waves are elastic waves that travel along the boundary of a structure and have been widely used for identifying damage in structures [1-5], detecting debonding in adhesively bonded structures [6-9], sensing liquid levels and properties [10-12], and assessing coatings on the substrate surface [13, 14]. The advantages of ultrasonic guided waves are that they can propagate for a long distance, enabling an efficient large-area inspection. Lamb waves

---

\* Corresponding author email: [alex.ng@adelaide.edu.au](mailto:alex.ng@adelaide.edu.au)

are guided waves in thin-walled structures, such as plates, shells, and pipes. When the plate is surrounded by air, Lamb waves are composed of multiple symmetric and anti-symmetric wave modes [15]. When one or both sides of the plate are exposed to liquid, there is a substantial increase in the energy leakage into the surrounding liquid medium [16, 17]. Therefore, guided waves in immersed plates are called leaky Lamb waves and they behave differently from their counterparts in the plates surrounded by air.

In addition to the symmetric and antisymmetric leaky Lamb wave modes, there is an interface mode called quasi-Scholte (QS) wave in the plate immersed in liquid [18]. Recently, studies have been conducted on the QS wave for a wide range of applications because of its ability to propagate along the plate-fluid interface over a long distance and high sensitivity to changes in the properties of both the plate and fluid. Tietze et al. [19] experimentally demonstrated that QS wave propagating at the interface between electrode and electrolyte is able to remove the diffusion boundary layer, which can be employed to accelerate the electrochemical process. Aubert et al. [20] invented a low-cost fluid manipulation device that employed the generation of QS wave to sort living cells and separate plasma from a blood microdroplet. Through schlieren imaging, the acoustic fields of the QS wave were experimentally visualized to be evanescent in the direction normal to the plate surface, which is a promising characteristic for microfluidic applications. Hayashi and Fujishima [21] experimentally confirmed that QS wave could be excited by applying the normal vibration directly on the surface of a plate loaded with water. The generated QS wave was shown to be sensitive to the change of the physical conditions on the plate surface. Thus, the QS wave is feasible for non-destructive testing (NDT) of water-filled storage tanks and pipes.

There are other studies focused on the application of QS wave, in which the QS wave is excited by mode conversion from the fundamental anti-symmetric mode ( $A_0$ ) of Lamb waves. Cegla et al. [18] developed a novel method for sensing fluid property by exciting guided waves on a plate that was partially immersed in the fluid. A transducer was attached at the end of the dry plate section (outside the fluid) to excite  $A_0$  wave. When the generated  $A_0$  wave traveled from the dry section of the plate to the section immersed in the fluid, part of the wave energy was reflected backward, and the rest of the wave energy was converted into the leaky  $A_0$  and QS waves. Leaky  $A_0$  wave decayed rapidly and disappeared after a short propagation distance. While QS wave propagated along the immersed plate with low attenuation, and then reached the end of the immersed section and reflected back to the measurement location. At the point where the plate was outside the fluid, the QS wave was converted back to  $A_0$  wave. The time-of-arrival and amplitude of the measured signals changed with the viscosity and bulk

longitudinal velocity of the fluid, and hence, they could be employed to measure the fluid properties. Yu et al. [22] proposed a Lamb wave-based method for assessing liquid levels in the nuclear cooling pipe system. The method used a pair of piezoelectric wafer transducers to be installed on the wall of a test tank. One of the transducers was used as an actuator and the other was used as a receiver. The wave signals were measured on the test tank filled with different amounts of water. It was found that the fundamental symmetric mode ( $S_0$ ) of Lamb waves was not influenced by the change of water level. In contrast, the presence of water significantly changed both the amplitude and phase of  $A_0$  wave. The phase change was shown to have a linear relationship with the change of water level. It should be noted that this study did not take into account the QS and leaky  $A_0$  waves, which also exist in the water-immersed plate [21, 23].

Guo et al. [24] developed two-dimensional (2D) finite element (FE) models to simulate guided wave propagation along an empty steel vessel and the steel vessel filled with water, respectively. At the selected excitation frequency,  $A_0$  and QS waves were identified on the water-free vessel and the water-filled vessel, respectively. The latter was found to propagate more slowly than the former. Therefore, the traveling time of the guided waves between two transducers could be also utilized for measuring the liquid level in the steel vessel. This study only considered a single excitation frequency, at which the leaky  $A_0$  wave mentioned in [18] was not detected in the water-immersed plate-like structure by both the 2D FE simulations and the experimental measurements [24].

The aforementioned studies employed the mode conversion between QS and  $A_0$  waves at different excitation frequencies to achieve different applications, where the interactions among various guided wave modes were shown to be different. To date, there are very limited studies on the variation with frequency of the mode conversion phenomenon. However, studying the influence of excitation frequency on guided wave propagation is very important because the behaviors of guided waves are frequency-dependent. For example, it was reported that the displacements of the QS wave mainly occur in the liquid, and the majority of studies on QS wave had been focused on the fluid properties sensing [10, 18]. Only in recent years, its applications were extended to detect damage for plate structures submerged in liquid due to the observation that the QS wave at low frequencies has most of its wave motions conserved in the immersed plate [21, 25]. QS wave is dispersive at low frequencies and becomes nondispersive at high frequencies. The wave structure of QS wave at a low frequency significantly differs from that at a high frequency. Between the high and low frequencies, there is a frequency range, at which QS wave transitions from dispersive to nondispersive. In this frequency range, the

wave structure of the QS wave changes rapidly with frequency, while that of the  $A_0$  wave does not change much. Therefore, the mode conversion between QS and  $A_0$  waves should also vary significantly with frequency, which has not been discussed in the literature.

In the present study, the frequency dependence of the mode conversion from  $A_0$  wave to QS wave is studied numerically and experimentally. The findings of this study complement the current knowledge about guided wave propagation in partially immersed plates and provide a guide on selecting appropriate excitation frequencies for NDT of partially immersed structures and assessing liquid properties and levels. The numerical method using a three-dimensional (3D) FE model is proposed to portray guided wave propagation in a steel plate, of which one side is partly exposed to water.  $A_0$  wave is excited at different frequencies on the dry section of the plate and travels to the immersed section. The simulation results provide a visualization of the interaction of guided wave modes in both the plate and water. Then, experiments are conducted on a steel tank that is partially filled with water. The time-space wave fields are captured by a scanning laser Doppler vibrometer (SLDV) before and after guided waves travel from the dry section of the plate into the immersed section. The mode conversion process is graphically shown with the use of 2D Fourier transform (FT). The experimental results show a good agreement with the numerical simulations. After that, the variation of the mode conversion from  $A_0$  wave to QS wave with the excitation frequency is analyzed based on the theoretical dispersion curves and mode shapes of guided waves. Furthermore, it is observed that the energy of guided waves can shift in the frequency domain during the mode conversion process if the phase velocity of the incident  $A_0$  wave is larger than the sound speed of the surrounding liquid medium. The energy shift in frequency can change the behaviors of guided waves, which should be paid attention to in practical applications.

The paper is organized as below. Section 2 compares the theoretical dispersion curves and mode shapes of guided waves in a plate surrounded by air and the plate with one side exposed to water. Section 3 describes the 3D FE model and presents the simulated guided wave fields in the partially immersed plate. After that, Section 4 shows the experimental setup and the configuration of measurement points. Section 5 illustrates the signal processing techniques and the analysis of experimentally measured signals. Then, Section 6 summarizes the frequency dependence of the mode conversion from  $A_0$  wave to QS wave and explains the mechanism of the energy shift in frequency phenomena according to the theoretical dispersion curves and mode shapes of the guided waves. Based on the findings, the selection of appropriate excitation frequency is discussed for reliable testing through the mode conversion from  $A_0$  wave to QS wave. Finally, conclusions are drawn in Section 7.

## 2. Guided waves in plates surrounded by air and plates with one side exposed to water

Guided waves behave differently in plates surrounded by air and plates immersed in water. When guided waves propagate in a plate in gaseous environments, there is a very small energy leakage from the plate to the air. The energy leakage to the air is not modeled in this study because the resistance of air to the displacements of particles at the plate surface is very small. As shown in Figure 1, traction-free boundary conditions are applied to the plate surface open to the air. In comparison, when one side of the plate is exposed to water, the out-of-plane displacements and stresses at the plate-water interface become continuous. The shear stresses are disconnected because water cannot sustain shear forces [26]. The energy leakage to the water layer is substantially larger than that to the air.

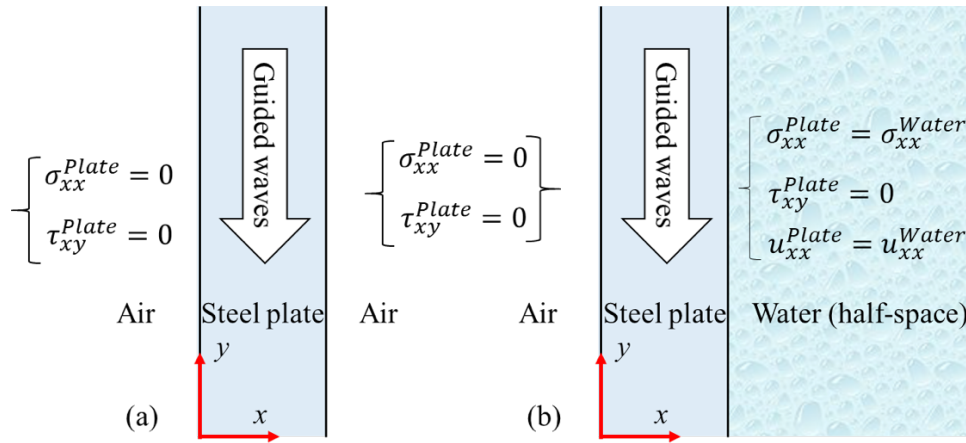


Fig. 1. Guided wave propagation models and boundary conditions for (a) a dry plate surrounded by air, and (b) a plate with one side exposed to water

The properties of guided waves vary with frequency, which can be theoretically predicted by dispersion curves. The present study employed the global matrix method to calculate the dispersion curves and the theoretical results were used to interpret the following numerical and experimental data. Two guided wave propagation models were constructed using the commercially available software DISPERSE [27]. They were a 2 mm thick steel plate and the plate with water loaded on one side, respectively. Table 1 gives the material properties of the steel plate and water. The water layer was defined as a semi-infinite half-space. The boundary conditions of the plate-air interface and plate-water interface were modeled by the solid-vacuum and solid-liquid interfaces, respectively. Based on the geometry and material properties, the stresses and displacements in the plate and water layers could be determined in

terms of the partial waves. Then, a global matrix equation representing the whole model was assembled by matching the boundary conditions of each interface. The global matrix equation is a function of frequency, wavenumber, and attenuation. Solving this global matrix equation gives a series of combinations of frequency, wave number, and attenuation, at which the partial waves can combine to a guided wave mode that propagates on the plates in the directions as shown in Figure 1.

Figure 2 compares the dispersion curves of guided waves for a 2 mm thick steel plate and the plate with water loaded on its one side. At the frequency range up to 500 kHz, only  $A_0$  and  $S_0$  waves exist in the plate without water. They are represented by the green and blue dash-dot lines in Figure 2, respectively. The black solid lines, red dashed lines, and magenta dotted lines denote QS, leaky  $A_0$ , and leaky  $S_0$  waves in the one-side water-immersed plate, respectively. The phase velocity  $C_p$  and the group velocity  $C_g$  can be related to the angular frequency  $\omega$  and the real wavenumber  $k$  as  $C_p = \omega/k$  and  $C_g = \partial\omega/\partial k$ . As shown in Figure 2(c), the wavenumber dispersion curves of  $A_0$  wave and  $S_0$  wave are almost overlapped with those of leaky  $A_0$  wave and leaky  $S_0$  wave, respectively. It should be noted that leaky  $A_0$  wave appears only after 150 kHz where its phase velocity is greater than the sound speed of the surrounding water [28]. At a frequency lower than 150 kHz, the wavenumber of QS wave in the one-side water-immersed plate (black solid line) is just slightly larger than that of  $A_0$  wave in the dry plate (green dash-dot line) and the difference between them increases with frequency.



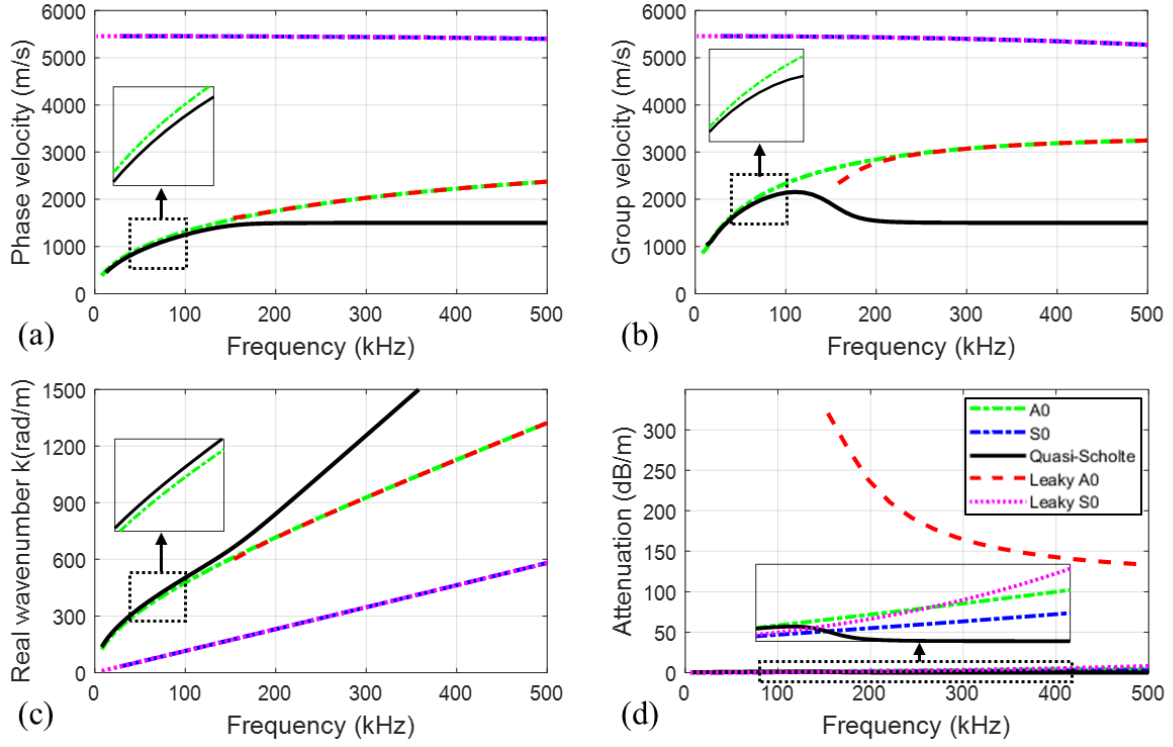


Fig. 2. Comparison of dispersion curves of a 2 mm thick steel plate and the plate with one side exposed to water: (a) phase velocity curves; (b) group velocity curves; (c) wavenumber curves; (d) attenuation curves (the legends in Figure 2(d) are applied for Figures 2(a)-(d)).

Figure 2(d) shows the attenuation dispersion curves where significant deviations can be observed between the dry plate and the one-side water-immersed plate. Obviously, leaky  $A_0$  wave (red dashed line) has a much higher attenuation than any other wave mode. This is because leaky  $A_0$  wave is dominated by the out-of-plane displacements so that the wave energy can easily and massively radiate into the surrounding water [29]. The attenuation dispersion curve of leaky  $A_0$  wave declines sharply in the selected frequency range. This means that the low-frequency leaky  $A_0$  wave has larger attenuation than the high-frequency leaky  $A_0$  wave. The levels of attenuation of other wave modes are close for the frequency lower than 200 kHz. Over 200 kHz, the attenuation of QS wave drops to almost zero, while the attenuations of  $A_0$ ,  $S_0$ , and leaky  $S_0$  waves slowly increase with frequency. From the above observations, it can be concluded that when guided waves propagate from the dry plate to the water-immersed plate,  $S_0$  wave is converted to leaky  $S_0$  wave that has the same wavenumber but slightly higher attenuation.  $A_0$  wave is converted to QS wave at a frequency lower than 150 kHz where both the wavenumber and attenuation of QS wave in the immersed plate are similar to those of  $A_0$  wave in the dry plate. However, leaky  $A_0$  wave appears when the excitation frequency exceeds

150 kHz.  $A_0$  wave can be mode converted to both QS wave and leaky  $A_0$  wave. Thus, the mode conversion process can be different with frequency.

The similarity between  $A_0$  wave in the dry plate and QS wave in the one-side water-immersed plate is also studied by their mode shapes. The mode shape of a guided wave mode shows the distributions of the displacements through the thickness of the structure and it can be calculated using DISPERSE [27]. The frequency band of interest is selected from 100 kHz to 200 kHz, in which the wavenumber dispersion curves of the  $A_0$  and QS waves gradually separate as the frequency increases. Figure 3 shows the mode shapes of  $A_0$  wave at 100 kHz, 150 kHz, and 200 kHz for the 2 mm thick steel plate that is not in contact with water. The deformation of the dry plate is dominated by out-of-plane displacements denoted by the blue solid lines. As the frequency increases, the mode shape diagrams of  $A_0$  wave do not display much difference.

Figure 4 shows the mode shapes of QS wave at 100 kHz, 150 kHz, and 200 kHz for the 2 mm thick steel plate with one side exposed to water. The water layer was defined as a semi-infinite half-space. As shown in Figure 4, the normalized displacement fields of the mode shapes in the water layer monotonically decrease with the distance away from the plate-water interface. To better compare the wave structures in the plate with and without water, the mode shape diagrams only show the 2 mm water regions near the plate-water interface. As shown in Figures 3(a) and 4(a), the deformation of QS wave in the immersed plate is similar to that of  $A_0$  wave in the dry plate when the frequency is lower than 150 kHz. However, the deformation in the immersed plate of QS wave decreases rapidly with frequency. At frequencies above 150 kHz, most of the displacements of QS wave occur in the water and the displacement fields in the immersed plate are very small (see Figures 4(b) and 4(c)). In general, when the frequency increases from 100 kHz to 200 kHz, QS wave changes significantly, while  $A_0$  wave remains almost unchanged. Therefore, it is expected that as the frequency increases, the mode conversion from  $A_0$  wave to QS wave should become more and more difficult since the similarity between the two wave modes reduces with frequency.

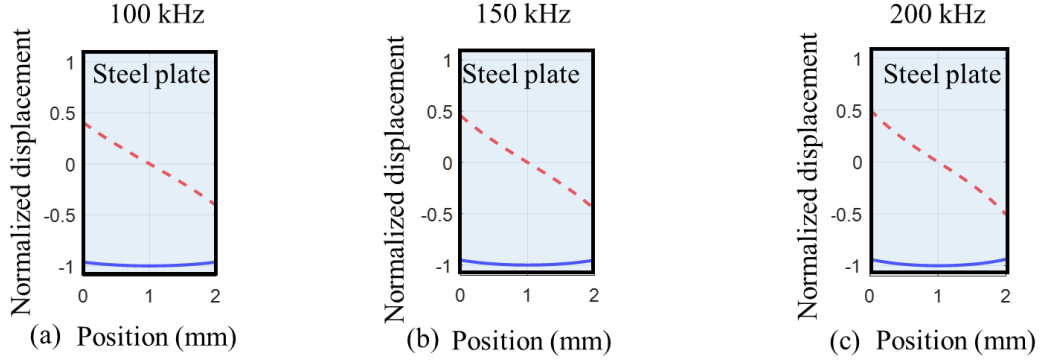


Fig. 3.  $A_0$  mode shapes for the 2 mm thick steel plate at (a) 100 kHz, (b) 150 kHz, and (c) 200 kHz (red dashed lines denote the in-plane displacements; blue solid lines denote the out-of-plane displacements)

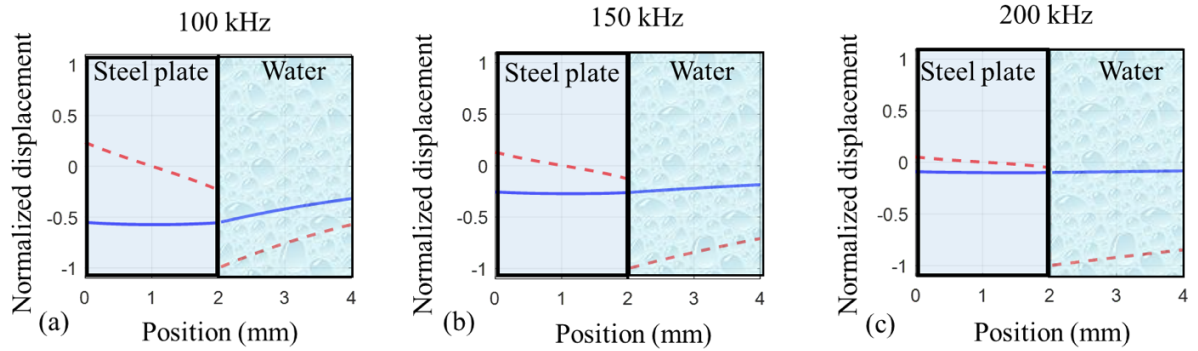


Fig. 4. QS mode shapes for the 2 mm thick steel plate with one side exposed to water at (a) 100 kHz, (b) 150 kHz, and (c) 200 kHz (red dashed lines denote the in-plane displacements; blue solid lines denote the out-of-plane displacements)

### 3. Numerical simulation of guided wave propagation

To portray the guided wave propagation in partially water-immersed plates, a 3D FE model was developed using the commercial FE software ABAQUS. Table 1 gives the material properties used for the FE simulation. A 300 mm  $\times$  150 mm  $\times$  2 mm steel plate was modeled with symmetry boundary conditions applied to the top and right edges and absorbing regions attached to the left and bottom edges, as shown in Figure 5. The absorbing regions were 50 mm wide and were divided into 50 layers. The mass-proportional damping of the material in the absorbing regions gradually increased layer by layer from zero at the innermost layer to  $4 \times 10^6$  at the outmost layer. The absorbing region by increasing damping can reduce unwanted waves reflected from the plate edges and has been widely used for ultrasonic guided wave simulation analysis [25, 30-33].

Table 1 Material properties of the steel and water

Material	Density ( $\text{kg m}^{-3}$ )	Young's modulus (GPa)	Poisson's ratio	Bulk modulus (GPa)	Bulk wave velocity ( $\text{m s}^{-1}$ )
Steel	7800	212.038	0.287	--	
Water	1000	--	--	2.2	1480

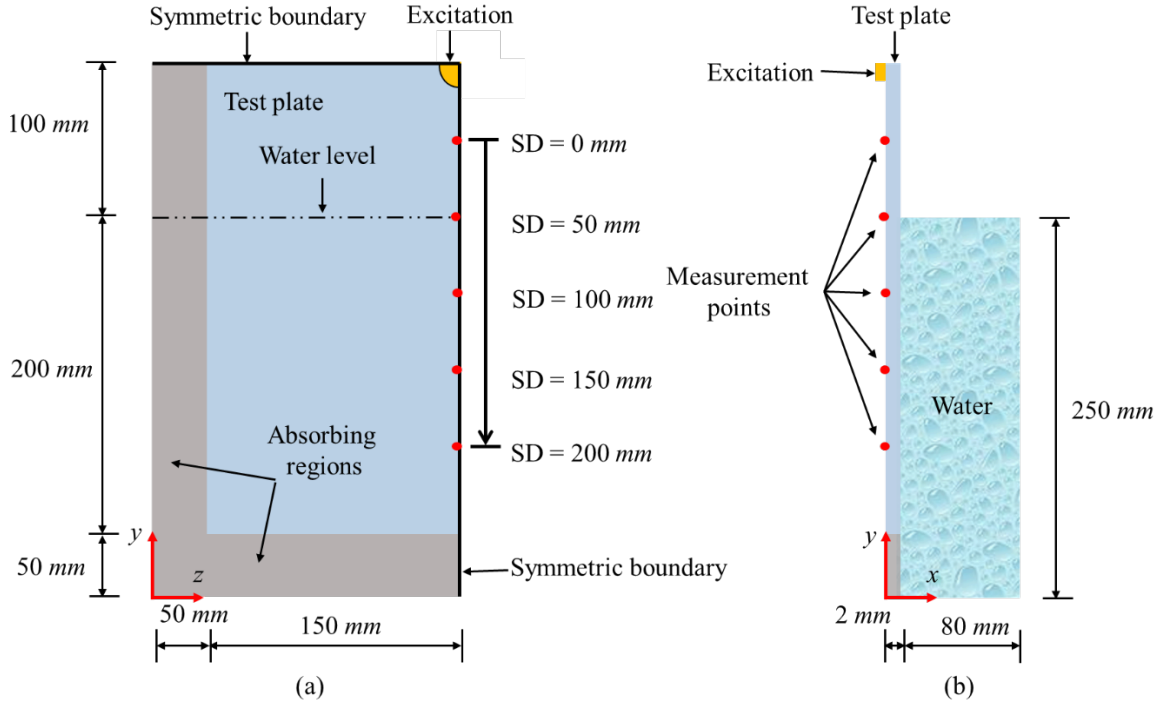


Fig. 5. Schematic diagram of the 3D FE model for a steel plate with one side partly exposed to water: (a) front view and (b) side view.

$A_0$  wave was generated by applying the out-of-plane displacements to the plate surface covered by a 5 mm diameter quarter-circle located at the top right corner of the plate [34]. Figure 9(b) shows the waveform of the excitation signal, which is a 10-cycle narrowband tone burst. To define the locations of the measurement points, a one-dimensional coordinate, scanning distance (SD), was defined along the right edge of the plate vertically downward as shown in Figure 5. The origin (SD = 0 mm) was set at the position of 50 mm below the excitation center. Then, the out-of-plane displacements were collected at five measurement points, which were evenly distributed at 50 mm apart from SD = 0 mm to SD = 200 mm. The other side of the plate was partially in contact with water as shown in Figure 5(b). The water level was located at the second measurement point (SD = 50 mm). The thickness of the water layer was chosen to separate the pressure wave reflections from the incident wave signals. The

steel plate and the water layer were meshed using 3D eight-node solid elements with reduced integration (C3D8R) and 3D eight-node acoustic elements with reduced integration (AC3D8R), respectively. The fluid and solid interface was simulated by node-surface tie constraints [16, 25]. The element size was set as 0.5 mm, which ensured approximately fifteen elements exist per wavelength of QS wave at 200 kHz. The simulation results were calculated using the central-difference integration by ABAQUS/Explicit [35].

Figure 6 presents the snapshots of the simulation results with the excitation frequency of 120 kHz. The color in the water regions denotes the acoustic pressure. At this excitation frequency, a large proportion of the QS wave energy is conserved in the one-side water-immersed plate, of which the deformation is similar to that of  $A_0$  wave in the dry plate as shown in Figures 3 and 4. When  $A_0$  wave travels from the dry section of the plate into the water-immersed section, part of the wave energy is converted to the pressure waves in the water, and the rest of the wave energy continues to propagate along the water-immersed plate at a speed slightly quicker than the pressure waves in the water. After a short propagation distance in the water-immersed plate, the first wave packet decays slowly and the acoustic field is tethered to the plate-water interface as shown in Figure 6(d). These are the typical characteristics of QS wave.

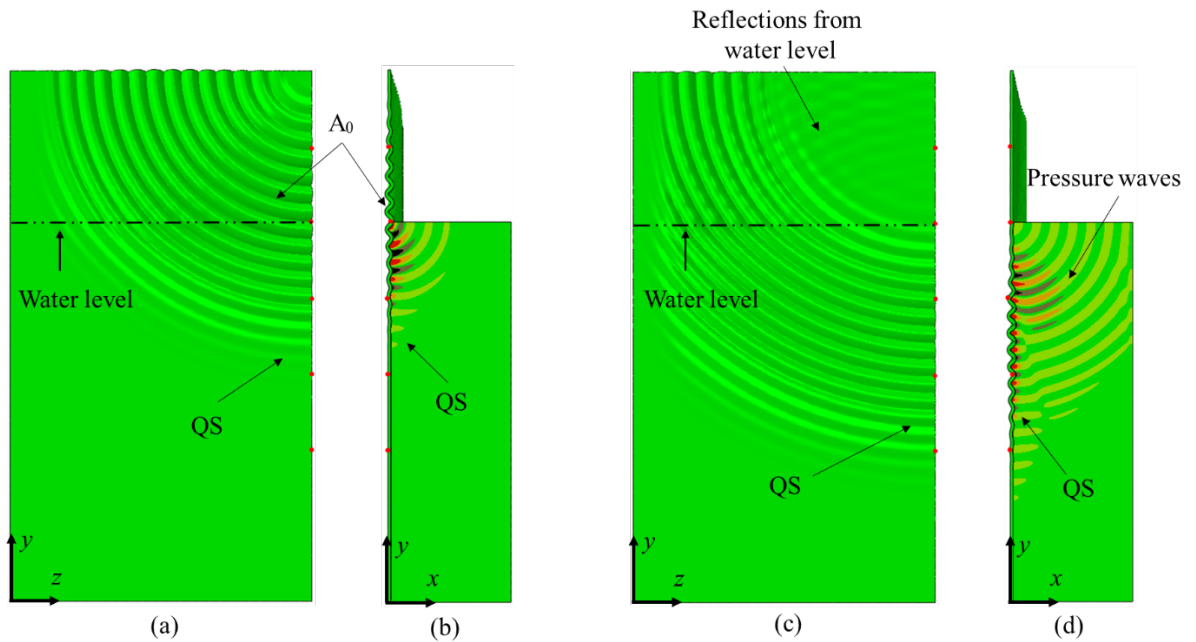


Fig. 6. Snapshots of the simulation results with the excitation frequency of 120 kHz (a) front view and (b) side view when the guided waves just travel from the dry section of the plate into

the water-immersed section; (c) front view and (d) side view after a short propagation distance in the water-immersed plate.

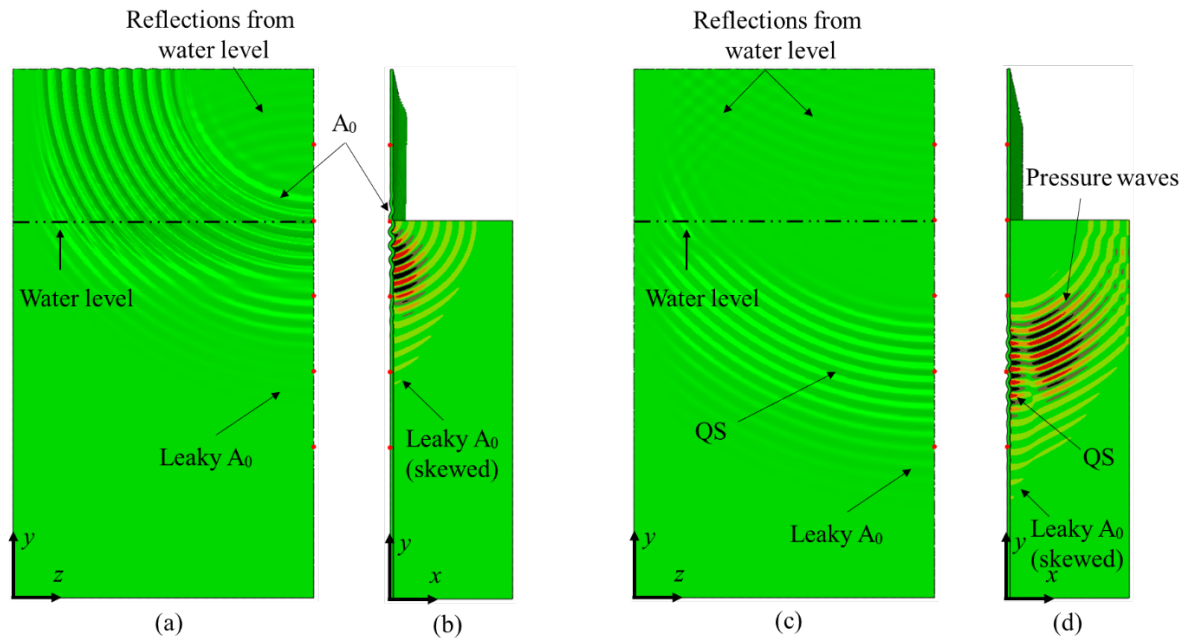


Fig. 7. Snapshots of the simulation results with the excitation frequency of 170 kHz (a) front view and (b) side view when the guided waves just travel from the dry section of the plate into the water-immersed section; (c) front view and (d) side view after a short propagation distance in the water-immersed plate.

Figure 7 shows the snapshots of the simulation results with the excitation frequency of 170 kHz. The mode shape of QS wave at 170 kHz is dominated by the in-plane displacements of water and the deformation of QS wave in the water-immersed plate is no longer similar to that of  $A_0$  wave in the dry plate (see Figures 3 and 4). The first wave packet in Figure 7 continuously radiates wave energy into the surrounding liquid medium, as shown by the skewed acoustic fields (skewed yellow lines) in the water layer in Figures 7(b) and 7(d). This wave packet with continuous wave energy leakage cannot be detected in Figure 6. Following the first wave packet, another wave packet propagates along the immersed plate at a speed slightly quicker than the pressure waves in water. Unlike the first wave packet, the second wave packet propagates with most of the energy confined to the plate-water interface. Based on the propagation speeds and the acoustic pressure in the water, the first and second wave packets in Figure 7 are identified as leaky  $A_0$  and QS waves, respectively.

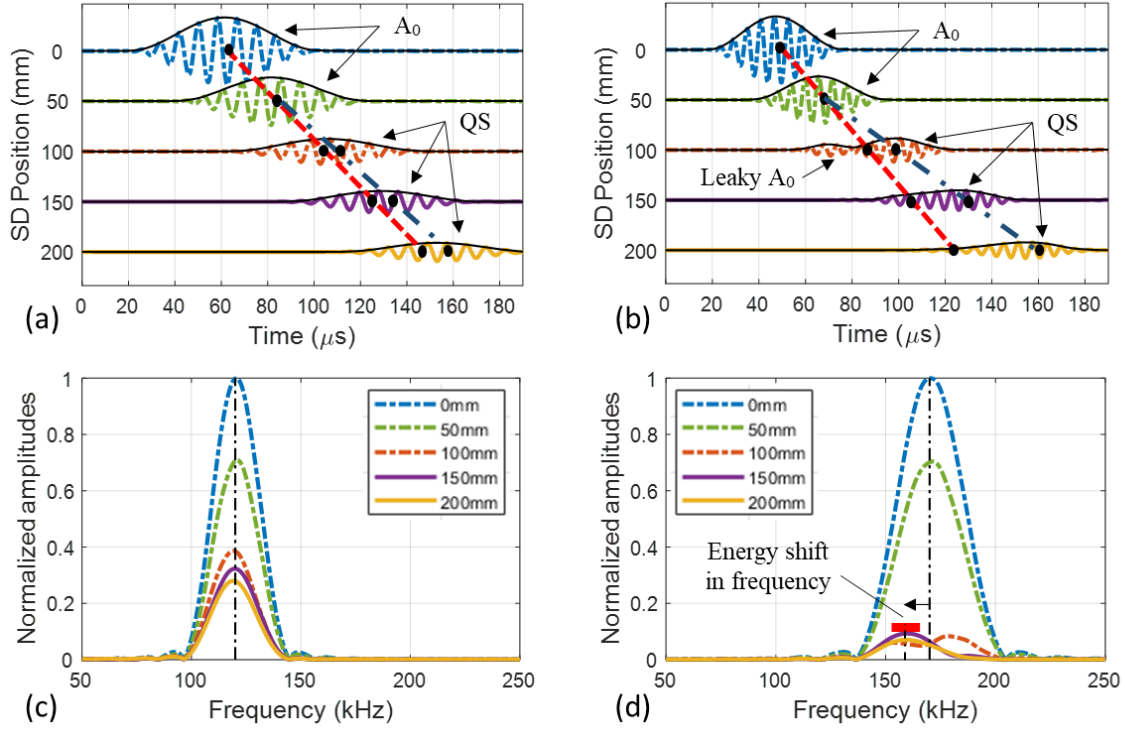


Fig. 8. Simulated time-domain signals for a steel plate with one side partly exposed to water (the same conditions as Case B presented in the experimental section) with the excitation frequency of (a) 120 kHz and (b) 170 kHz, respectively; (c) and (d) are the frequency spectrums of (a) and (b), respectively (the time-domain signals measured at SD = 100 mm, 150 mm, and 200 mm in Figure 8(b) are magnified by a factor of four).

To better observe how the signals change with the propagation distance, Figure 8 presents the simulated out-of-plane displacements at the five measurement points that are denoted by the red dots in Figure 5. Figures 8(a) and 8(b) show the time-domain data for the excitation frequencies of 120 kHz and 170 kHz, respectively. Their corresponding frequency spectrums are given in Figures 8(c) and 8(d), respectively. The amplitudes are normalized by the maximum absolute amplitudes of the signals measured at the first measurement point (SD = 0 mm). It should be noted that when the excitation frequency is 170 kHz, the time-domain signals measured at SD = 100 mm, 150 mm, and 200 mm are so small that they are magnified by a factor of four and shown in Figure 8(b). The normalized amplitudes of the signals collected in the immersed section of the plate (SD > 50 mm) significantly decrease with the excitation frequency. In addition, when the excitation frequency is 170 kHz, the simulated signals show apparent frequency shifts in the frequency spectrums. For example, the central frequency of the signal measured at SD = 100 mm, denoted by the orange dash-dot line in Figure 8(d), shifts to a frequency slightly higher than the central excitation frequency of 170 kHz. Subsequently,

the wave energy shifts to a lower frequency as shown by the signals measured at  $SD = 150$  mm (purple solid line) and  $SD = 200$  mm (yellow solid line) in Figure 8(d). The simulation results demonstrate that the guided wave propagation in the partially water-immersed plate varies significantly with the excitation frequency. The following sections present experimental investigations to validate the simulation results, and the phenomenon of energy shift in the frequency domain due to the presence of water is discussed in detail.

#### 4. Experiment setup

Experiments were conducted on a steel tank, of which the front wall was used as the test plate. The test plate was 2 mm thick and made of mild steel. A circular piezoceramic wafer (Ferroperm Pz27, Denmark) was used as the guided wave actuator and it was bonded on the external surface of the test plate as indicated by the PZT transducer in Figure 9(a). The diameter and the thickness of the piezoceramic wafer were 5 mm and 2 mm, respectively. An arbitrary function generator (AFG 2021, China) was used to generate the excitation signal. Figure 9(b) gives the waveform of the excitation signal that is a 10-cycle narrowband tone burst. The excitation signal was magnified by a voltage amplifier (Krohn-Hite 7500, USA), and then sent to the piezoceramic wafer transducer.

An SLDV (Polytec PSV-400-M2-20, Germany) was used to collect the experimental signals. The silver-white paint on the plate surface in Figure 9(a) is the reflective paint (CRC, USA) that was sprayed on the scan area to increase the reflection of the laser beam. Next to the scan area, a ruler was placed to assist with defining measurement points. Then, the out-of-plane displacements were recorded by the SLDV at a sampling rate of 10.24 MHz. Each measurement was improved by averaging the signals with 800 acquisitions and applying a low-pass filter with the cut-off frequency being 1MHz. Figure 9(c) shows the schematic diagram of the experiment setup.



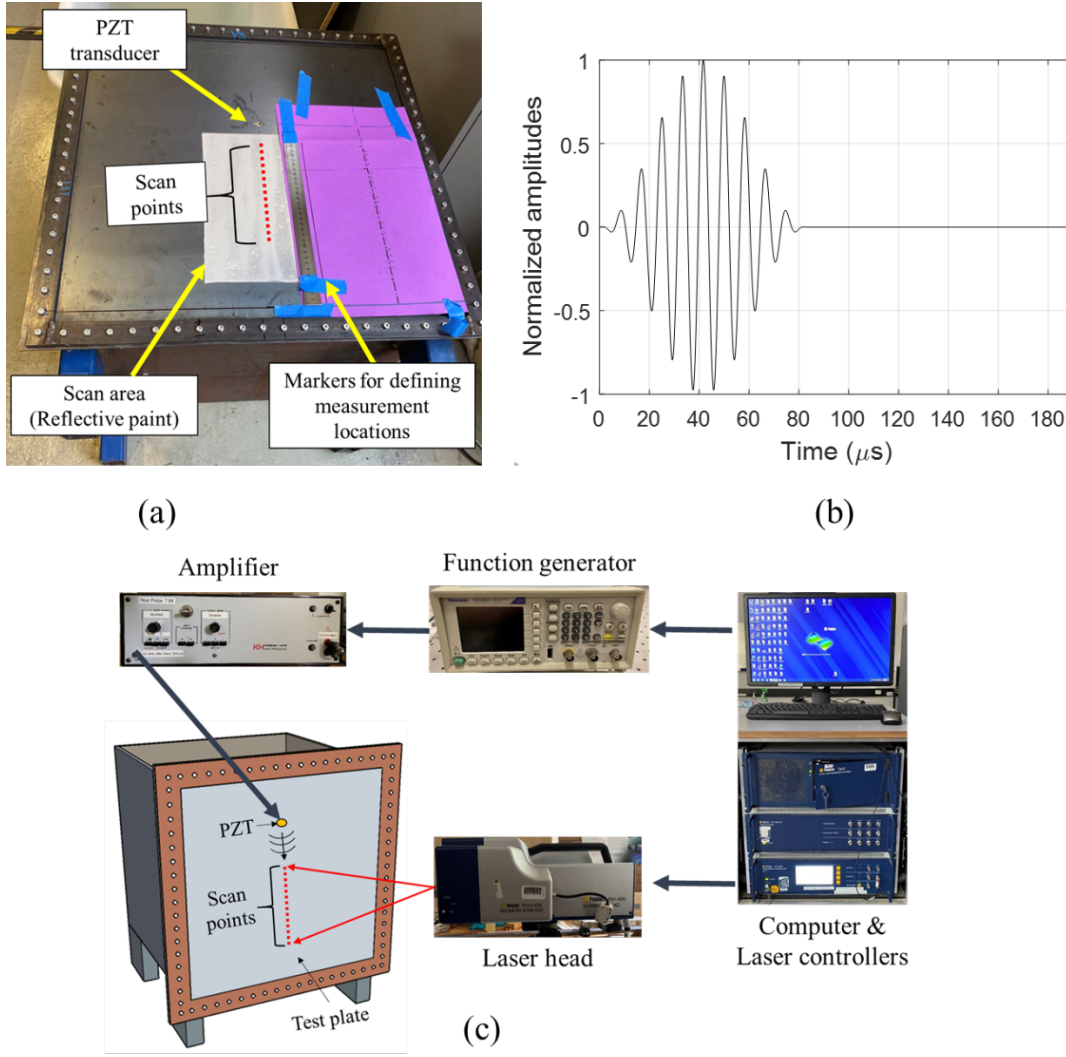


Fig. 9. (a) A photo of the metal tank, (b) the waveform of the excitation signal, and (c) the experiment setup

Similar to the 3D FE model, a one-dimensional coordinate,  $SD$ , was defined on the external surface of the test plate. The origin ( $SD = 0$  mm) was set at the position of 50 mm vertically below the center of the piezoceramic wafer. The experimental study included two parts, which were five-point scan tests and line scan tests, respectively. Firstly, the five-point scan tests were conducted on the steel tank to validate the simulation results. The signals were measured at  $SD = 0$  mm, 50 mm, 100 mm, 150 mm, and 200 mm, which were at the same locations as the simulations as shown in Figure 5.

Then, line scan tests were carried out to visualize guided wave fields on the test plate. The objective of the line scan test was to experimentally demonstrate the interaction of each guided wave mode during the mode conversion process. According to the simulation results shown in Figures 6, 7, and 8, the mode conversion process mainly occurs between  $SD = 50$

mm and  $SD = 150$  mm. After  $SD = 150$  mm, only the QS wave can be detected as shown by the signals measured at  $SD = 150$  mm and  $SD = 200$  mm in Figure 8. Therefore, the line scan tests focused on the region between  $SD = 0$  mm and  $SD = 150$  mm as shown in Figure 10(a). The signals were collected at 127 measurement points, which were evenly distributed along the scan line from  $SD = 0$  mm to  $SD = 150$  mm. With these measurements, the time-space wave fields could be constructed by plotting the amplitudes of the measured signals versus time and  $SD$ .

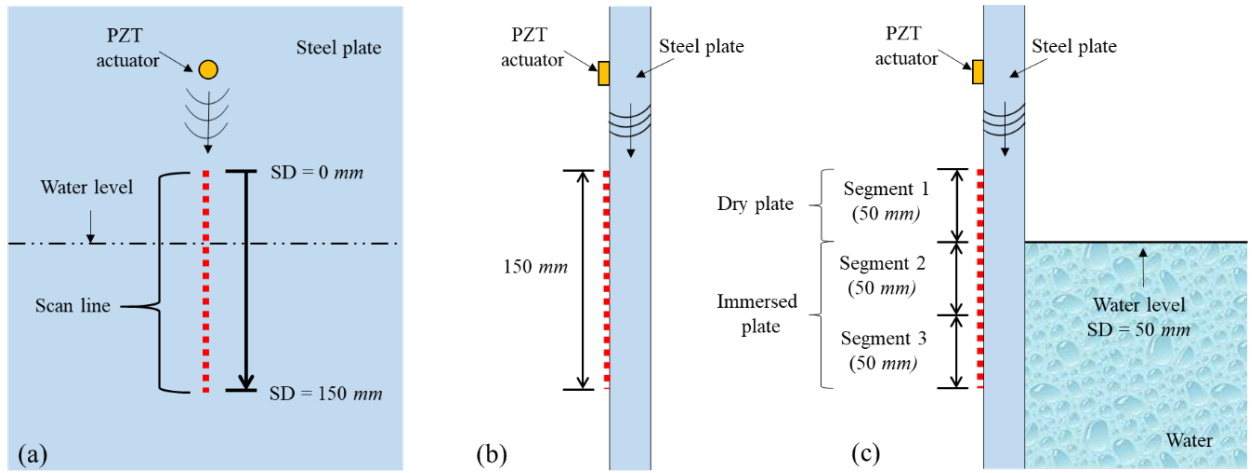


Fig. 10. Schematic diagram of the scan line on the test plate (a) front view; (b) side view of Case A (empty tank); (c) side view of Case B (partially water-filled tank).

In order to demonstrate the influence of water on the guided wave propagation, both the five-point scan tests and line scan tests were carried out on the empty tank (Case A) and the partially water-filled tank (Case B), respectively. Figures 10(b) and 10(c) show the side view of the scan line on the test plate for Case A and Case B, respectively. In Case B, the steel tank was partially filled with water with the water level set at  $SD = 50$  mm. Therefore, one-third of the scan line was located in the non-immersed section of the plate (from  $SD = 0$  mm to  $SD = 50$  mm), called “dry plate”, and the rest of the scan line was located in the section of the one-side water-immersed plate (from  $SD = 50$  mm to  $SD = 150$  mm), which was denoted as “immersed plate”. Guided waves were generated on the test plate by the piezoceramic wafer located at 100 mm above the water level. The time-space wave fields were captured before and after guided waves traveled from the dry plate into the immersed plate.

## 5. Experimental results and analysis

### 5.1 Validation of numerical simulations

This section presents the experimental measurements to validate the accuracy of the 3D FE model. Figure 11 presents the experimental results with the central excitation frequency of 120 kHz. Figures 11(a) and 11(b) show the time-space wave fields for the empty tank and the partially water-filled tank, respectively. The amplitudes are normalized by the maximum absolute amplitudes of the signals measured at the first scan point ( $SD = 0$  mm). The black dashed line in Figure 11(b) denotes the water level located at  $SD = 50$  mm. The generated guided wave fields in the dry section of the plate (between  $SD = 0$  mm and  $SD = 50$  mm) are similar for both the empty tank in Figure 11(a) and the partially water-filled tank in Figure 11(b). However, the amplitudes of the signals measured in the immersed plate ( $SD > 50$  mm) of the partially water-filled tank in Figure 11(b) are smaller than their counterparts in the empty tank in Figure 11(a). This indicates that part of the wave energy leaks from the immersed plate into the water as shown in the snapshots of the simulation results (see Figures 6(a) and 6(b)).

Figures 11(c) and 11(d) show typical examples of the signals measured at  $SD = 0$  mm, 50 mm, 100 mm, 150 mm, and 200 mm for the empty tank and the partially water-filled tank, respectively. The wave speed in the immersed plate of the partially water-filled tank, as denoted by the dark blue dash-dot line in Figure 11(b), is slightly slower than the wave speed in the dry plate that is marked by the red dashed line. From the wave speed evaluation, the wave packets measured from the empty tank in Figure 11(a) and the dry section of the partially water-filled tank in Figure 11(b) are identified as  $A_0$  wave [24].  $S_0$  wave can be not observed because it has negligible out-of-plane motions at the selected excitation frequency [25, 36]. The changes of the wave speed and amplitude in the immersed section of the test plate demonstrate that  $A_0$  wave is mode converted to QS wave. Figures 11(e) and 11(f) present the frequency spectrums of Figures 11 (c) and 11(d), respectively. The amplitudes are normalized by the signal measured at the first scan point ( $SD = 0$  mm). The peaks of all measured signals are concentrated around the central frequency of the excitation signal of 120 kHz. There is a good agreement between the experimental measurements shown in Figures 11 (d) and 11(f) and the simulation results (see Figures 8(a) and 8(c)).

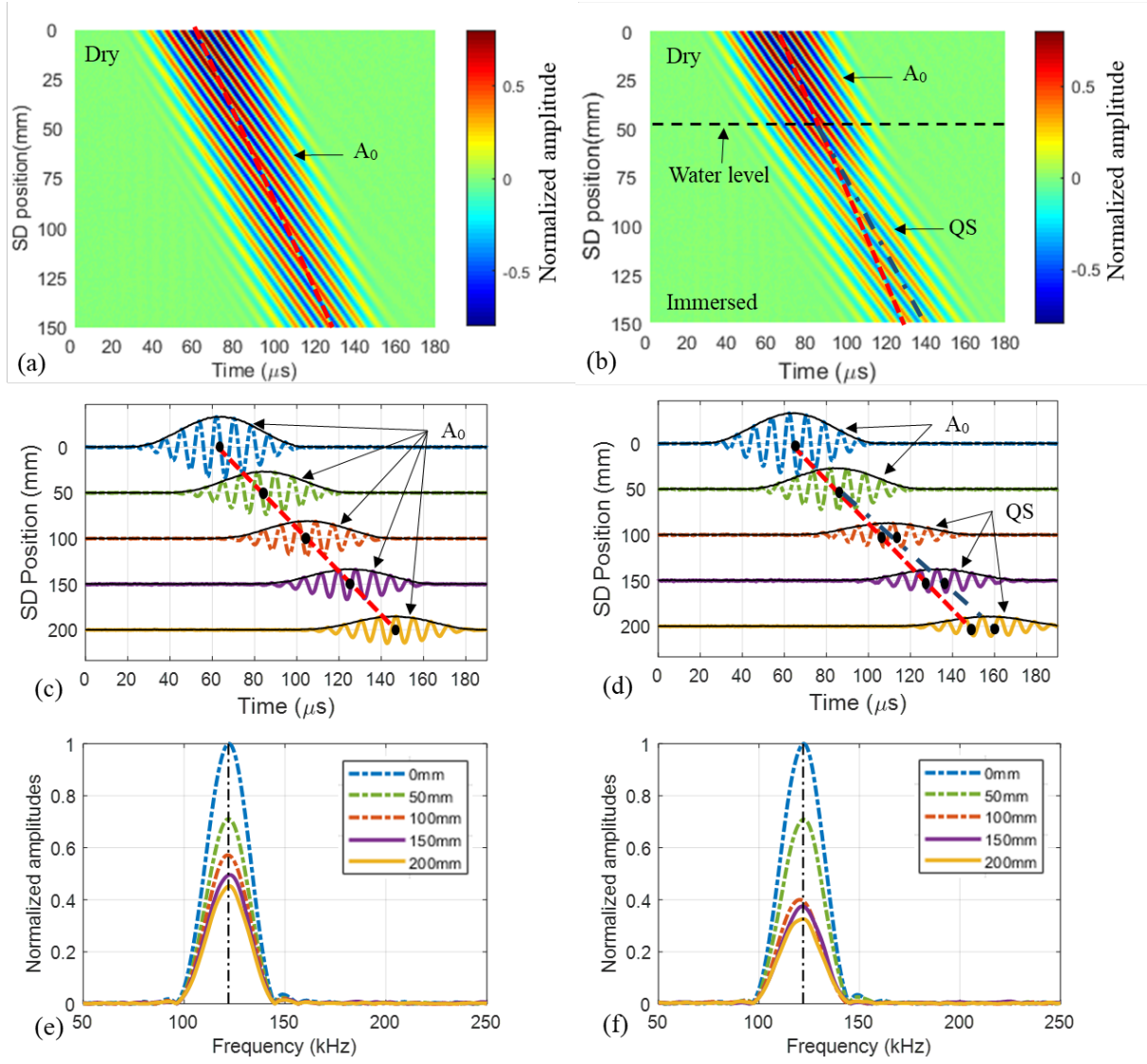


Fig. 11. Experimental results with the excitation frequency of 120 kHz: (a) and (b) are time-space wave fields for the empty tank and the partially water-filled tank, respectively; (c) and (d) are the typical examples of the time-domain signals for the empty tank and the partially water-filled tank, respectively; (e) and (f) are the frequency spectrums of (c) and (d), respectively.

For comparison, Figure 12 presents the experimental results with the central excitation frequency of 170 kHz. Figures 12(a) and 12(b) present the time-space wave fields for the empty tank and the partially water-filled tank, respectively. For the empty tank, the waves propagate at a consistent speed as represented by the red dashed line in Figure 12(a). The same wave fields are observed in the dry section of the plate ( $SD < 50$  mm) of the partially water-filled tank as shown in Figure 12(b). However, when guided waves propagate into the water-immersed section ( $SD > 50$  mm), the wave amplitudes decrease rapidly and reach the minimum

between  $SD = 80$  mm and  $SD = 90$  mm as indicated in Figure 12(b). After that, the waves slightly increase in amplitude near the position of  $SD = 100$  mm, and then continue to propagate at a speed (dark blue dash-dot line) that is much slower than the original speed of the waves in the dry plate (red dashed line).

Figures 12(c) and 12(d) show typical time-domain signals measured at  $SD = 0$  mm, 50 mm, 100 mm, 150 mm, and 200 mm for the empty tank and the partially water-filled tank, respectively. To provide better observation of the signals, the measured signals from the partially water-filled tank at  $SD = 100$  mm, 150 mm, and 200 mm are magnified by a factor of four and shown in Figure 12(d). Guided waves propagate as a single wave packet along the dry section of the plate (between  $SD = 0$  mm and  $SD = 50$  mm). However, after a short propagation distance in the immersed plate, the signal measured at  $SD = 100$  mm shows two wave packets, each propagating at different speeds. It should be noted that the mode split phenomenon is not observed on the water-immersed plate with the central excitation frequency of 120 kHz (see Figure 11(d)). The first wave packet decays quickly and disappears as shown by the signal measured at  $SD = 150$  mm in Figure 12(d), while the second wave packet propagates with low attenuation at a slower wave speed (dark blue dash-dot line). Figures 12(e) and 12(f) show the frequency spectrums of Figures 12(c) and 12 (d), respectively. The signals measured at  $SD = 100$  mm, 150 mm, and 200 mm from the partially water-filled tank in Figures 12(f) have much smaller amplitudes than their counterparts from the empty tank in Figures 12(e). In addition, Figure 12(f) displays the energy shift in frequency, which has a good agreement with the simulation results (see Figure 8(d)). It is confirmed that the energy shift in the frequency domain is due to the presence of water because this phenomenon does not occur in the case of the empty tank as shown in Figure 12(e).

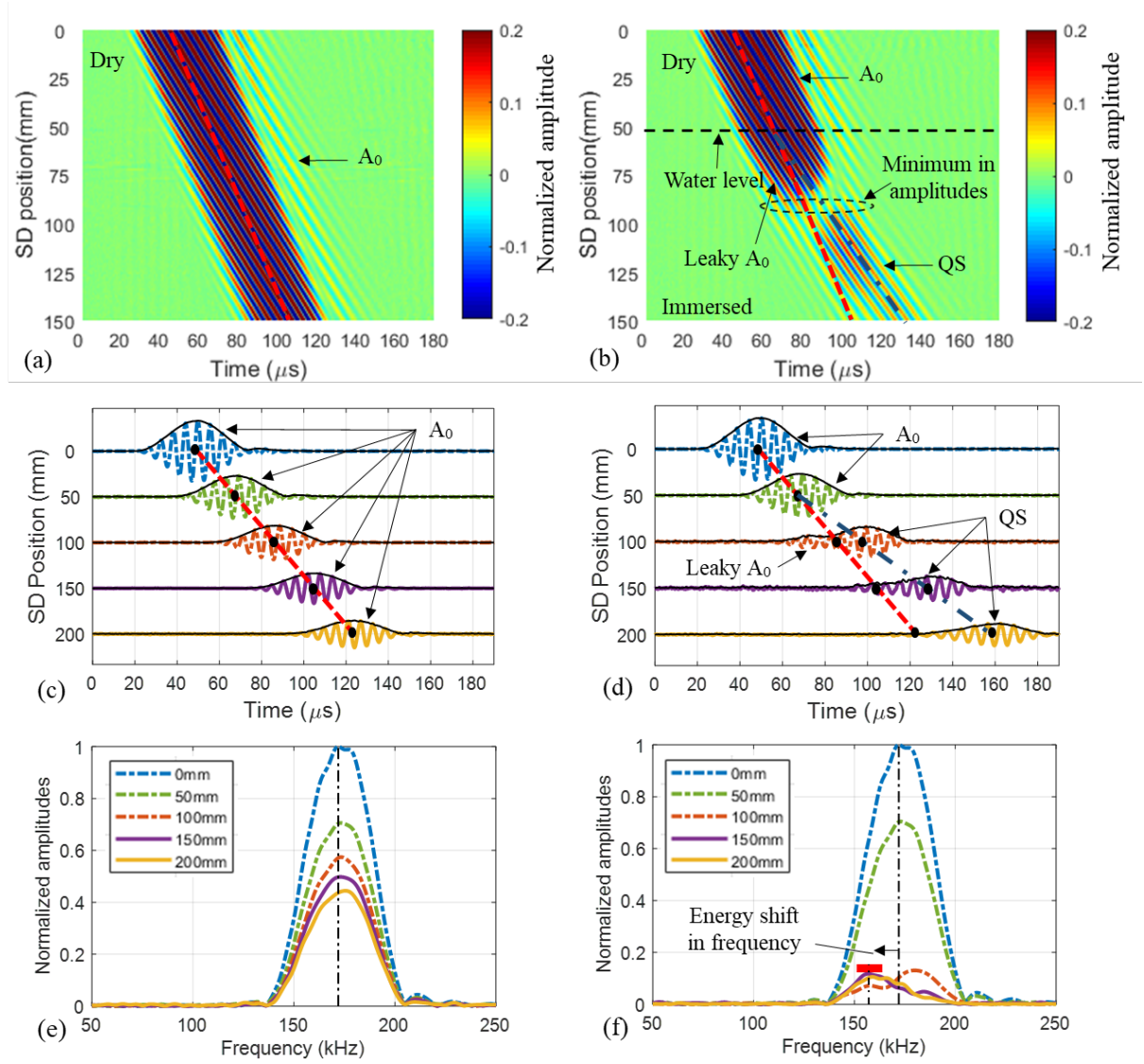


Fig. 12. Experimental results with the excitation frequency of 170 kHz: (a) and (b) are time-space wave fields for the empty tank and the partially water-filled tank, respectively; (c) and (d) are the typical examples of the time-domain signals for the empty tank and the partially water-filled tank, respectively; (e) and (f) are the frequency spectrums of (c) and (d), respectively (the time-domain signals measured at SD = 100 mm, 150 mm, and 200 mm in Figure 12(d) are magnified by a factor of four).

To further investigate the accuracy of the 3D FE model, Figure 13 compares the peak amplitudes of the simulated and experimentally measured signals in the frequency domain for both the empty tank (Case A) and the partially water-filled tank (Case B), respectively. The magnitudes are normalized by their corresponding peak amplitudes of the signals measured at SD = 0 mm. Figures 13(a) and 13 (b) present the results with the excitation frequency of 120 kHz and 170 kHz, respectively. In the dry section of the plate (SD < 50 mm), the amplitudes



of the simulated and experimentally measured signals are identical for both cases. When guided waves just pass the water level (from  $SD = 50$  mm to  $SD = 100$  mm), the measured signals of Case A decrease slowly and smoothly, but the signal amplitudes of Case B drop substantially. After  $SD = 100$  mm, the guided wave amplitudes in both Case A and Case B decrease slowly with distance. When the excitation frequency increases from 120 kHz to 170 kHz, the amplitudes of the signals of Case A do not show obvious changes as shown by the red hexagons and circles in Figures 13. However, the amplitudes of the signals of Case B significantly decrease when the excitation frequency increases. In general, the proposed 3D FE model well predicts the frequency shift phenomena and wave attenuation characteristics and hence, the simulation results are validated to interpret the experimental data.

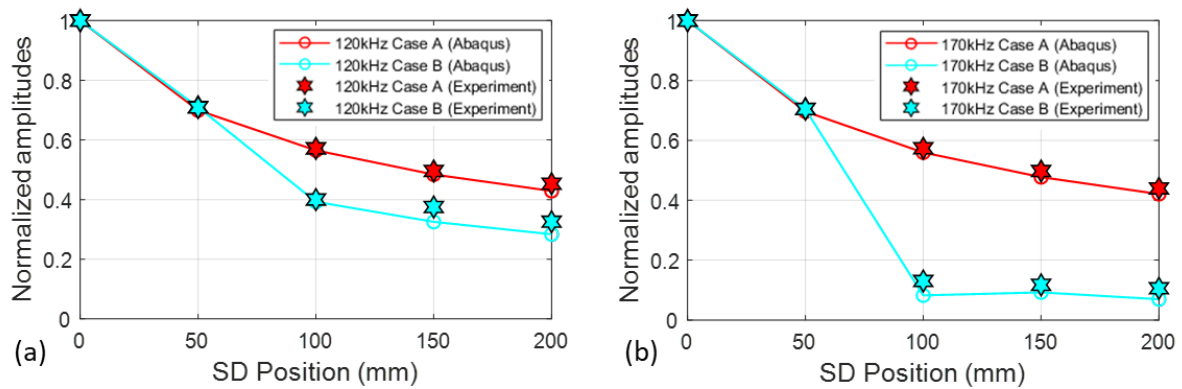


Fig. 13. Normalized amplitudes of the simulated and experimentally measured signals in the frequency domain for the empty tank (Case A) and the partially water-filled tank (Case B) with the excitation frequency of (a) 120 kHz and (b) 170 kHz, respectively.

## 5.2 Segmented frequency wavenumber analysis

Although the time-space analysis displays the variation of wave amplitudes with the time and propagation distance, it cannot determine the wave mode conversion characteristics such as mode identities and their corresponding frequency components. To graphically demonstrate the mode conversion process, 2D FT is employed to identify the mode information of the experimental data collected along the scan line on the partially water-filled tank (Case B). The scan line is divided into three segments, each of which is 50 mm long and comprises 43 measurement points as shown in Figure 10(c). The generated guided waves first propagate through Segment 1 (Dry plate) and then to Segment 2 (Water-immersed plate) and finally to Segment 3 (Water-immersed plate). The water level is between Segment 1 and 2. The time-

space data of each segment is converted to the frequency-wavenumber spectrum through 2D FT, which is defined as:

$$\mathbf{u}(k, f) = \iint \mathbf{u}(x, t) e^{-i(2\pi ft - kx)} dt dx \quad (1)$$

where  $\mathbf{u}(k, f)$  and  $\mathbf{u}(x, t)$  are the data in the frequency-wavenumber domain and time-space domain, respectively.  $k$  and  $f$  denote the wavenumber and frequency, respectively.  $x$  and  $t$  represent the space and time coordinate, respectively.

Figures 14(a)-14(c) present the experimentally measured data in the time-space domain for the three segments and their corresponding frequency-wavenumber spectrums are given in Figures 14(d)-14(f), respectively. The excitation frequency is 120 kHz. The color in the frequency-wavenumber spectrums denotes the wave energy of the experimentally measured signals, which is calculated by 2D FT. The black solid lines are the theoretical wavenumber dispersion curves of  $A_0$ ,  $S_0$ , and QS waves calculated by DISPERSE. As mentioned in Section 2, the wavenumber dispersion curves of leaky  $A_0$  and leaky  $S_0$  waves overlap with  $A_0$  and  $S_0$  waves. For convenience, leaky  $A_0$  and leaky  $S_0$  waves are labeled as  $A_0$  and  $S_0$  in the figures, respectively. In Segment 1, where the plate is not immersed in water, only the energy of  $A_0$  wave is identified in the frequency-wavenumber spectrum as shown in Figure 14(d). The energy of  $S_0$  wave is absent because it has negligible out-of-plane displacements [25, 36]. Next, the wave energy is converted from  $A_0$  wave to QS wave immediately in Segment 2 as shown in Figure 14(e). The mode conversion occurs rapidly and the energy of QS wave decays slowly with distance and dominates the frequency-wavenumber spectrums of Segments 2 and 3. At this excitation frequency, leaky  $A_0$  wave is not detected and the energy shift in frequency is not observed.

The measured data with the central excitation frequency of 170 kHz is shown in Figure 15. Only  $A_0$  wave is identified in Segment 1 as shown in Figures 15(a) and 15(d). When  $A_0$  wave just propagates into the water-immersed plate, most of the wave energy is converted to leaky  $A_0$  wave that has the same wavenumber as  $A_0$  wave as shown in Figures 15(b) and 15(e). The signals measured between  $SD = 50$  mm and  $SD = 80$  mm are dominated by leaky  $A_0$  wave whose amplitude decays rapidly. In the meantime, QS wave is also generated as the amplitude slowly increases with propagation distance until leaky  $A_0$  wave nearly disappears at the end of Segment 2. Leaky  $A_0$  wave and QS wave have different wavenumbers and phase velocities (see Figure 2). Therefore, The minimum wave amplitudes between  $SD = 80$  mm and  $SD = 90$



mm can be caused by the destructive interference between the Quasi-Scholte wave and leaky  $A_0$  wave.

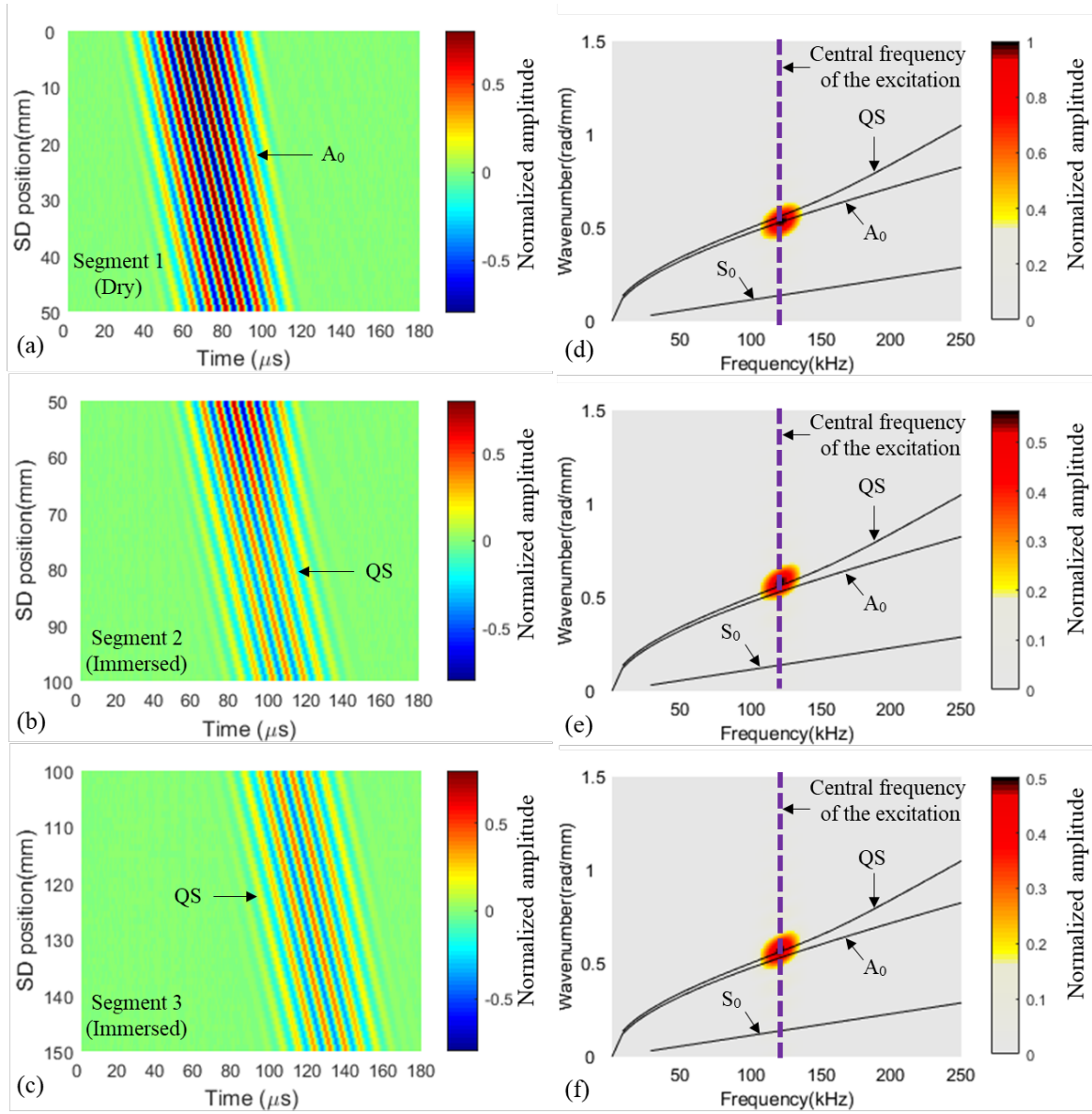


Fig. 14. Experimental results for the partially water-filled tank with the central excitation frequency of 120 kHz: time-space wave fields for (a) Segment 1, (b) Segment 2, and (c) Segment 3, respectively; frequency wavenumber spectrums for (d) Segment 1, (e) Segment 2, and (f) Segment 3, respectively.

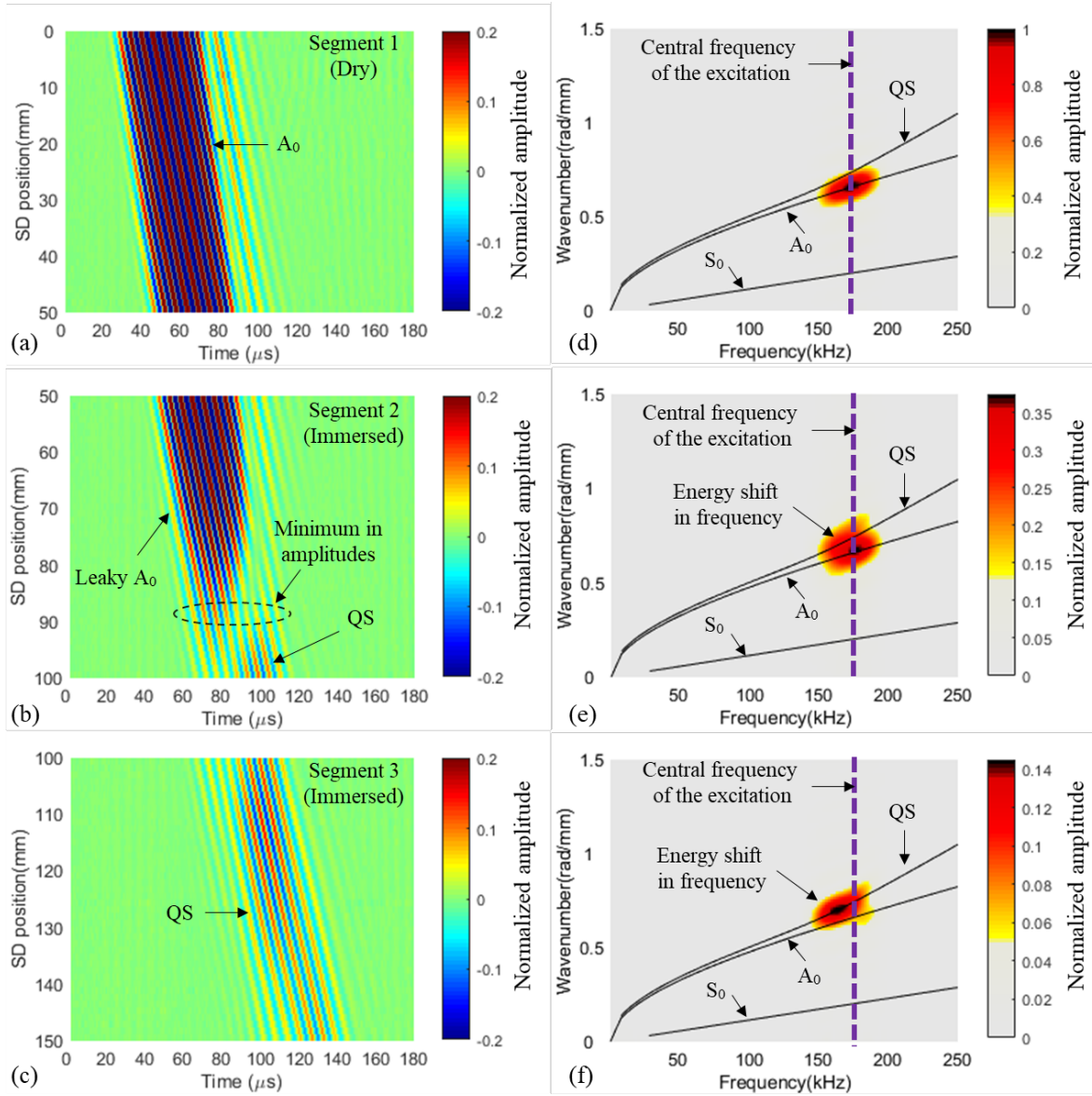


Fig. 15. Experimental results for the partially water-filled tank with the central excitation frequency of 170 kHz: time-space wave fields for (a) Segment 1, (b) Segment 2, and (c) Segment 3, respectively; frequency wavenumber spectrums for (d) Segment 1, (e) Segment 2, and (f) Segment 3, respectively.

After that, the wave fields in Segment 3 are dominated by only QS wave (see Figures 15(c) and 15(f)). The energy of the mode converted QS wave concentrates at a frequency slightly lower than the central excitation frequency of 170 kHz, which agrees well with Figures 8(d) and 12(f). Therefore, conclusions can be drawn that at the intersection between the dry plate and immersed plate,  $A_0$  wave is mode converted to both QS wave and leaky  $A_0$  wave with more energy transferred to the latter. Leaky  $A_0$  wave that has mostly out-of-plane displacements in the plate continuously radiates compressional waves in the liquid and also

excites QS wave. Considering that the deformation in the immersed plate of QS wave at low frequencies is greater than that at high frequencies (see Figure 4), the anti-symmetrical excitation of leaky  $A_0$  wave is more likely to produce QS wave at lower frequencies. This can be also manifested by the frequency spectrums (see Figures 8(d) and 12(f)) where the wave energy is progressively transferred from a higher frequency at  $SD = 100$  mm to a frequency lower than the central excitation frequency at  $SD = 150$  mm. After that, the wave energy is conserved at the frequency (lower than the excitation frequency of 170 kHz) and propagates with small attenuation.

### 5.3 Further study by sweeping the excitation frequency

To further investigate the phenomenon of energy shift in the frequency domain, the five-point scan tests were conducted on the partially water-filled tank using the excitation signals with the central frequencies of 110 kHz, 130 kHz, 140 kHz, 150 kHz, 160 kHz, and 180 kHz. The collected signals were transformed to the frequency domain and shown in Figure 16. The amplitudes were normalized by the signals measured at the first scan point ( $SD = 0$  mm). As it is confirmed from the segmented frequency wavenumber plots (see Figures 14 and 15), the signals measured at  $SD = 150$  mm to 200 mm, denoted by the purple and yellow solid lines in Figures 11(f), 12(f), and 16, are dominated by the low-attenuation QS wave. Therefore, it can be concluded that the normalized amplitude of QS wave converted by  $A_0$  wave decreases when the excitation frequency increases.

For excitation frequencies below 140 kHz, the signals measured from both the dry section and water-immersed section of the plate are concentrated around the central excitation frequency (see Figure 11(f) and Figures 16(a)-16(c)). The energy shift in frequency can be observed for excitation frequencies over 150 kHz, where leaky  $A_0$  wave appears as the phase velocity of the incident  $A_0$  wave becomes larger than the sound speed of the surrounding water. Under the central excitation frequency of 150 kHz and 160 kHz, the signals measured at  $SD = 100$  mm, 150 mm, and  $SD = 200$  mm have most of their wave energy concentrated at a frequency lower than the central excitation frequency (see Figure 16(d) and 16(e)). The range of the frequency shift also increases when the central excitation frequency increases. However, the signals measured at  $SD = 100$  mm under the central excitation frequency of 170 kHz and 180 kHz are shown to have more energy conserved at higher frequencies (see Figure 12(f) and Figures 16(f)). This is because the amplitudes of QS wave converted by  $A_0$  wave are so small that leaky  $A_0$  wave can be detected clearly at this measurement point. Leaky  $A_0$  wave at higher frequencies decays more slowly than that at lower frequencies as discussed in Section 2,

making the central frequency of the signal shift to a relatively higher frequency. However, leaky  $A_0$  wave completely disappears after a short propagation distance, and only QS wave can be detected at  $SD = 150$  mm and  $SD = 200$  mm, as shown in Figure 15. Since the low-attenuation QS wave at lower frequencies has a larger deformation fraction in the immersed plate, the measured signals from the surface of the immersed plate eventually concentrate at a frequency lower than the central excitation frequency. The next section summarizes the frequency dependence of the mode conversion from  $A_0$  wave to QS wave and further explains the mechanism of the frequency shift phenomena.

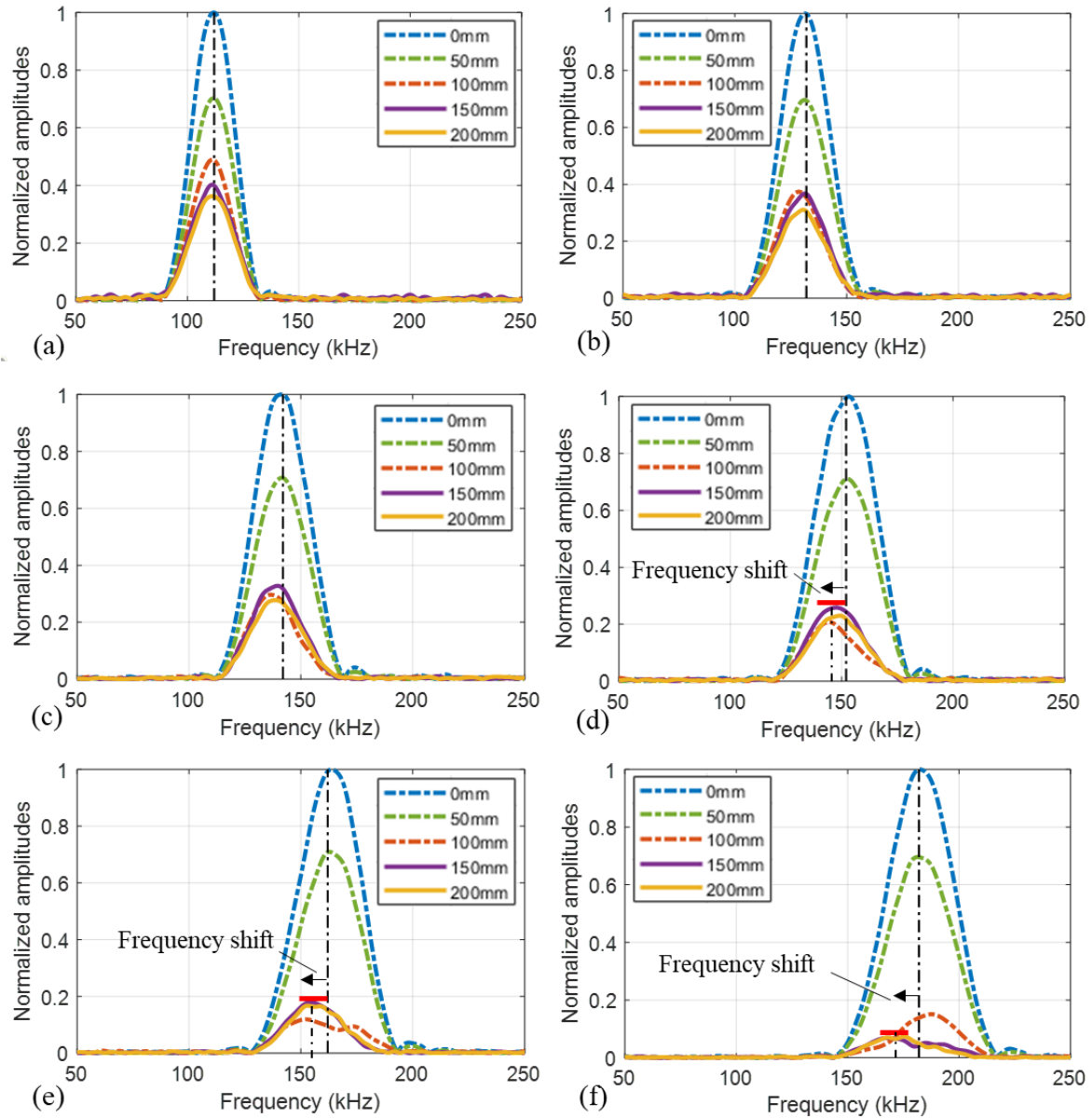


Fig.16. Frequency spectrums of the signals experimentally measured from the partially water-filled tank with the excitation frequency of (a) 110 kHz; (b) 130 kHz; (c) 140 kHz; (d) 150 kHz; (e) 160 kHz; and (f) 180 kHz.

## 6. Discussion and application

### 6.1 The influence of excitation frequency on the mode conversion process

The mode conversion from  $A_0$  wave to QS wave has been numerically and experimentally shown to be dependent on the excitation frequency. The frequency dependence is summarized in this section and analyzed according to the dispersion behaviors of the guided waves. The theoretical dispersion curves and mode shapes of guided waves have been derived from the global matrix theory and are present in Section 2. In the following discussion, the term “high frequency” means the frequency range, in which the phase velocity of the incident  $A_0$  wave is larger than the sound speed of the surrounding liquid medium and the leaky  $A_0$  wave appears. The term “low frequency” indicates the frequency range, in which the phase velocity of the incident  $A_0$  wave is smaller than the sound speed of the surrounding liquid medium and the quasi-Scholte wave is dispersive. The transition frequency between the high and low frequency ranges can be estimated from the phase velocity dispersion curves. For example, the phase velocity of  $A_0$  wave for a metallic plate monotonically increases with frequency until it reaches the Rayleigh wave speeds, which is around 3000 m/s for steel. The sound speed of water is around 1500 m/s, which is constant for all frequencies. Therefore, the transition frequency is around 150 kHz, at which the phase velocity of  $A_0$  wave traveling along the 2 mm thick steel plate is around 1500 m/s, as shown in Figure 2(a). The phase velocity dispersion curves can be calculated by the commercial software DISPERSE. The input data includes the material properties of the plate, the plate thickness, and the sound speed of the surrounding liquid medium.

At low frequencies, the difference in wavenumber between  $A_0$  wave and QS wave is small. In addition, the deformation of QS wave in the immersed plate is similar to that of  $A_0$  wave in the dry plate (see Figures 3 and 4). Thus,  $A_0$  wave can be mode converted to QS wave rapidly with most of the wave energy conserved in the plate. When the excitation frequency increases, the energy distribution of QS wave in the immersed plate decreases sharply and the similarity reduces between  $A_0$  and QS waves (see the dispersion curves in Figure 2 and mode shapes diagrams in Figures 3 and 4). Therefore, the amplitude of QS wave converted by  $A_0$  wave significantly decreases with frequency.

At high frequencies, leaky  $A_0$  wave appears when the phase velocity of the incident  $A_0$  wave becomes larger than the sound speed of the water.  $A_0$  wave is mode converted to both QS wave and leaky  $A_0$  wave with more energy transferred to the latter. Leaky  $A_0$  wave that has

the flexural mode shape in the plate continuously radiates compressional waves in the liquid and also excites QS wave. After a short propagation distance, leaky  $A_0$  wave decays quickly and disappears so that only QS wave can be detected.

## **6.2 The mechanism of the energy shift in frequency phenomenon**

The energy shift in frequency occurs during the mode conversion process when the incident  $A_0$  wave is generated at high frequencies. The mechanism of the energy shift in frequency phenomenon can be explained by the dispersion curves and the mode shapes of guided wave modes as follows.

Firstly, the central frequency of the signal can shift to a frequency higher than the center frequency of the excitation, when the wave fields are dominated by the leaky  $A_0$  wave (see signals at  $SD = 100$  mm in Figures 12(f) and 16(f)). This is due to the fact that the attenuation dispersion curve of leaky  $A_0$  wave declines sharply in the selected frequency region (see Figure 2). The low-frequency components of leaky  $A_0$  wave decay much quicker than the high-frequency components. Therefore, leaky  $A_0$  wave at high frequencies can travel longer distances, making the central frequency of the signals measured in the immersed plate near the water level relatively higher than the central excitation frequency.

Secondly, the central frequency of the mode converted QS wave is relatively lower than the center frequency of the excitation. One reason is that the deformation in the immersed plate of QS wave at low frequencies has a flexural mode shape, which is similar to  $A_0$  wave in the dry plate. But the similarity between QS and  $A_0$  waves reduces with frequency. This makes the mode conversion from  $A_0$  wave to QS wave (at the intersection of the dry plate and the water-immersed plate) much easier at low frequencies than that at high frequencies, with more energy transferred and conserved in the plate. The other reason is that the deformation of QS wave in the plate is rapidly reduced with frequency (see Figure 4). Thus, QS wave at low frequencies can be excited on the plate more easily by the out-of-plane motions of leaky  $A_0$  wave after guided waves propagate into the water-immersed plate. Since the generated QS wave has low attenuation, the measured signals in the immersed plate eventually shift to a frequency lower than the central excitation frequency (see signals at  $SD = 150$  mm and  $SD = 200$  mm in Figure 12(f) and Figures 16(d)-(f)).

### 6.3 Implications for practical applications

The findings of the present study suggest that the low-attenuation QS wave can be easily excited by mode conversion from  $A_0$  wave that is generated at low frequencies on the dry plate section. This phenomenon can be employed to detect damage for the plate structures that are partially immersed in liquid, such as partially water-filled tanks and pipelines. These structures generally experience uniform corrosion and pitting corrosion. The latter is more critical because it damages the deep structures with little loss of metal [37].

Previous studies have characterized corrosion damage using  $A_0$  wave for plates surrounded by air [38-40] and QS wave for plates in contact with liquid [21, 41]. For partially immersed plates, it is also possible to evaluate the defects by sending  $A_0$  waves on the dry section of the plate and measuring the QS wave signals on the immersed section. This method is very promising for long-range inspection because QS wave does not radiate energy in the liquid (see Figures 6 and 7) and is able to travel along the plate-fluid interface with low attenuation. The measurement range through using the dispersive QS wave by mode conversion from  $A_0$  wave can be of the order of several meters based on the low attenuation characteristics as shown in Figure 13. However, the actual propagation distance is dependent on the material properties of the plate and the surrounding liquid medium as well as the excitation frequency. As discussed in Section 6.1, the lower the excitation frequency, the more wave energy conserved in the plate during the mode conversion process, and therefore the longer the propagation distance. Another advantage is that this method has the potential to characterize the structural defects entirely based on the QS wave, which is appealing for accurate detection and imaging of the defects [42]. After a short propagation distance, leaky  $A_0$  wave decays quickly and disappears due to high attenuation. The low-attenuation QS wave can be well separated from the leaky  $S_0$  wave, of which the propagation speed is three times that of QS wave (see Figure 2(b)). Although leaky  $S_0$  wave has low attenuation, it is not sensitive enough to identify small and shallow corrosion damage in the early stage [43-45]. In contrast, the QS wave has the shortest wavelength at a given frequency and provides better sensitivity than the leaky  $S_0$  wave to shallow hidden corrosion pits in immersed plates [41].

It should be noted that the damage detection algorithm for the partially immersed structures should consider the change of wave behaviors due to the mode conversion phenomenon and the presence of liquid. It is recommended to select an excitation frequency below the transition frequency, at which the proposed phenomenon of guided wave energy shift in frequency can be avoided. (see Figure 11 and Figure 14). Otherwise, the effect of the

potential wave energy shift in the frequency domain should also be carefully considered and compensated. For instance, it is observed in the present study that the wave energy of the mode converted QS wave in the immersed plate moves to a frequency below the central excitation frequency, making the actual wavenumber of the QS wave smaller than that at the central excitation frequency (see Figure 15(f)). This also indicates a smaller phase velocity, a higher group velocity, and a larger wavelength (see Figure 2). The change of the propagation characteristics of guided waves will affect the performance of conventional damage detection and imaging algorithms [16, 46].

The mode conversion between QS and  $A_0$  waves in partially immersed plates was widely used for liquid-level assessing [22, 24, 47] and fluid-property sensing [18, 48, 49]. The behaviors of  $A_0$  wave depend on the geometry and material properties of the plate, while QS wave reflects the properties of both the plate and the surrounding fluid medium. Generally, the difference between QS and  $A_0$  waves becomes larger with frequency. Therefore, increasing the excitation frequency can result in larger deviations in the signals measured from the partially immersed plate in terms of the time of arrival, amplitude, and phase angle, and hence, it can potentially increase the sensitivity of the signals to the variation of liquid level and fluid properties. However, the results of the present study show that the amplitude of the QS wave converted by  $A_0$  wave significantly decreases with frequency. Therefore, the optimal excitation frequency is a trade-off between the sensitivity and the amplitudes of the measured signals. For simplicity, it is also recommended to excite the guided waves at a low frequency to ensure that the phase velocity of the incident  $A_0$  wave is smaller than the sound speed of the surrounding liquid medium. Without the interference of the leaky  $A_0$  wave, the mode conversion process is simple and the frequency shift phenomena can be avoided.

Lastly, QS wave at high excitation frequencies becomes nondispersive and is promising for fluid manipulation [20] and removing diffusion boundary layer [19, 50], where the focus is directed on the movement of the fluid particles and the deformation in the plate is not interested. The low-attenuation QS wave with most of the wave energy concentrated at the plate-fluid interface has the potential to cover a large area of the fluid near the plate surface. However, attention should be paid to the potential frequency shift of the measured signals. As shown in Figures 15 and 16, guided wave energy can shift in the frequency domain during the mode conversion process, which gives rise to the change of wave behavior such as group and phase velocities.



## 7. Conclusion

This paper has provided an insight into the measurement of ultrasonic guided waves in partially immersed plates. The main contributions are concluded as follows:

- (1). Global matrix method is employed to derive the theoretical dispersion curves and modes shapes of guided waves for a 2 mm thick steel plate and the plate with one side loaded with water. It is found that the low-frequencies QS wave in the one-side water-immersed plate and the  $A_0$  wave in the dry plate have similar wavenumbers and deformations. But the similarity reduces with frequency.
- (2). A 3D FE model is developed to simulate the guided wave field in the steel plate with one side partially immersed in water. The simulation results are validated by the experimental data. The frequency shift phenomenon and the guided wave amplitudes with propagation distance can be well predicted.
- (3). The experimental studies are conducted on the empty tank and the partially water-filled tank, respectively. It is confirmed that the frequency shift phenomenon is due to the presence of water. The further investigation presents a segmented frequency wavenumber analysis to graphically demonstrate the mode conversion process, which is divided into three segments: (i) before guided waves propagate into the water-immersed plate, (ii) guided waves just propagate into the water-immersed plate, and (iii) after a short propagation distance in the water-immersed plate. The experimental data are compared with the theoretical dispersion curves, through which the mode identities and the corresponding experimentally measured wave energy can be determined.
- (4). The guided wave energy shift in the frequency occurs during the mode conversion process, which is not caused by the material nonlinearity (micro cracks) of the plate. The amplitudes of the guided wave signals measured from the water-immersed plate section are much smaller than those obtained from the water-free plate section, on which the frequency shift phenomenon is not observed. Then, the mechanism of the energy shift in frequency phenomenon is explained by the attenuation dispersion curves of leaky  $A_0$  wave and the mode shapes of QS wave.
- (5). Based on the findings, the selection of appropriate excitation frequency is discussed for damage detection of partially submerged structures, assessing liquid properties and levels, and fluid manipulations.

In summary, comprehensive investigations have been carried out for the frequency dependence of the mode conversion from  $A_0$  wave to QS wave in a steel plate with one side

partially immersed in water. The findings can provide supports for the further development of guided wave-based techniques for damage detection on partially immersed structures, liquid-level assessing, and fluid-property sensing. This paper has only focused on the plate partially immersed in water. Future work can study the partially immersed structures with different geometries and investigate the effect when the structure is immersed in other types of liquid. In addition, the influence of damage such as corrosion pits or stress cracking on the guided wave propagation and mode conversion can be investigated.

## **8. Acknowledgment**

This work was funded by the Australia Research Council (ARC) under grant numbers DP200102300 and DP210103307. The authors are grateful for this support.

## **9. References**

- [1] J. Moll, C.P. Fritzen, Guided waves for autonomous online identification of structural defects under ambient temperature variations, *Journal of Sound and Vibration*, 331 (2012) 4587-4597.
- [2] J. He, C.A.C. Leckey, P.E. Leser, W.P. Leser, Multi-mode reverse time migration damage imaging using ultrasonic guided waves, *Ultrasonics*, 94 (2019) 319-331.
- [3] A. Aseem, C.T. Ng, Debonding Detection in Rebar-reinforced Concrete Structures Using Second Harmonic Generation of Longitudinal Guided Wave, *NDT & E International*, (2021) 102496.
- [4] S. He, C.-T. Ng, C. Yeung, Time-Domain Spectral Finite Element Method for Modeling Second Harmonic Generation of Guided Waves Induced by Material, Geometric and Contact Nonlinearities in Beams, *International Journal of Structural Stability and Dynamics*, 20 (2020) 2042005.
- [5] Y. Choi, S.H. Abbas, J.-R. Lee, Aircraft integrated structural health monitoring using lasers, piezoelectricity, and fiber optics, *Measurement*, 125 (2018) 294-302.
- [6] M. Liu, S. Chen, Z.Z. Wong, K. Yao, F. Cui, In situ disbond detection in adhesive bonded multi-layer metallic joint using time-of-flight variation of guided wave, *Ultrasonics*, 102 (2020) 106062.
- [7] K. Wang, M. Liu, Z. Su, S. Guo, F. Cui, Mode-mismatching enhanced disbond detection using material nonlinearity in guided waves at low frequency, *Journal of Sound and Vibration*, 490 (2021) 115733.
- [8] B. Zima, R. Kędra, Baseline-free debonding detection in reinforced concrete structures by elastic wave propagation, *Measurement*, 172 (2021) 108907.
- [9] X. Hong, Y. Liu, Y. Liufu, P. Lin, Debonding Detection in Hidden Frame Supported Glass Curtain Walls Using the Nonlinear Ultrasonic Modulation Method with Piezoceramic Transducers, *Sensors*, 18 (2018) 2094.
- [10] O. Önen, Dispersion and Sensitivity Analysis of Quasi-Scholte Wave Liquid Sensing by Analytical Methods, *Journal of Sensors*, 2017 (2017).

- [11] R. Kazys, L. Mazeika, R. Sliteris, R. Raisutis, Measurement of viscosity of highly viscous non-Newtonian fluids by means of ultrasonic guided waves, *Ultrasonics*, 54 (2014) 1104-1112.
- [12] X. Hong, B. Zhang, Y. Liu, Z. Zhou, M. Ye, H. Qi, Liquid level detection in porcelain bushing type terminals using piezoelectric transducers based on auto-encoder networks, *Measurement*, 141 (2019) 12-23.
- [13] S. Tietze, F. Singer, S. Lasota, S. Ebert, J. Landskron, K. Schwuchow, K.S. Drese, G. Lindner, Monitoring of Soft Deposition Layers in Liquid-Filled Tubes with Guided Acoustic Waves Excited by Clamp-on Transducers, *Sensors*, 18 (2018) 526.
- [14] M. Schmitt, K. Schmidt, S. Olfert, J. Rautenberg, G. Lindner, B. Henning, L.M. Reindl, Detection of coatings within liquid-filled tubes and containers by mode conversion of leaky Lamb waves, *J. Sens. Sens. Syst.*, 2 (2013) 73-84.
- [15] J.L. Rose, *Ultrasonic guided waves in solid media*, Cambridge university press, 2014.
- [16] J. Chen, Z. Su, L. Cheng, Identification of corrosion damage in submerged structures using fundamental anti-symmetric Lamb waves, *Smart Materials and Structures*, 19 (2009) 015004.
- [17] J. Chen, Z. Su, L. Cheng, The medium coupling effect on propagation of guided waves in engineering structures and human bone phantoms, *Coupled systems mechanics*, (2012).
- [18] F.B. Cegla, P. Cawley, M.J.S. Lowe, Material property measurement using the quasi-Scholte mode—A waveguide sensor, *The Journal of the Acoustical Society of America*, 117 (2005) 1098-1107.
- [19] S. Tietze, M. Reißweber, J. Schlemmer, G. Lindner, Investigation of the Surface Condition of an Electrode after Electropolishing under the Influence of Surface Acoustic Waves, *Physics Procedia*, 70 (2015) 1039-1042.
- [20] V. Aubert, R. Wunenburger, T. Valier-Brasier, D. Rabaud, J.-P. Kleman, C. Poulain, A simple acoustofluidic chip for microscale manipulation using evanescent Scholte waves, *Lab on a Chip*, 16 (2016) 2532-2539.
- [21] T. Hayashi, R. Fujishima, Defect Detection Using Quasi-Scholte Wave for Plate Loaded with Water on Single Surface, *Materials Transactions*, (2016) M2016204.
- [22] L. Yu, B. Lin, Y.-J. Shin, J. Wang, Z. Tian, Ultrasonic gas accumulation detection and evaluation in nuclear cooling pipes, *SPIE*, 2012.
- [23] Z. Tian, L. Yu, Lamb wave structural health monitoring using frequency-wavenumber analysis, in: *AIP Conference Proceedings*, AIP, 2013, pp. 302-309.
- [24] P. Guo, B. Deng, X. Lan, K. Zhang, H. Li, Z. Tian, H. Xu, Water Level Sensing in a Steel Vessel Using A0 and Quasi-Scholte Waves, *Journal of Sensors*, 2017 (2017).
- [25] X. Hu, C.-T. Ng, A. Kotousov, Scattering characteristics of quasi-Scholte waves at blind holes in metallic plates with one side exposed to water, *NDT & E International*, 117 (2021) 102379.
- [26] L. Yu, Z. Tian, Case study of guided wave propagation in a one-side water-immersed steel plate, *Case Studies in Nondestructive Testing and Evaluation*, 3 (2015) 1-8.
- [27] B. Pavlakovic, M. Lowe, *Disperse user manual: a system for generating dispersion curves*, Copyright B Pavlakovic, M Lowe, (2003).
- [28] E. Glushkov, N. Glushkova, O. Miakisheva, Analytically based study of ultrasonic sounding of an immersed plate: hidden mode A0 and backward leaky waves, *Proceedings of Meetings on Acoustics*, 38 (2019) 065008.
- [29] P. Rizzo, J.-G. Han, X.-L. Ni, Structural health monitoring of immersed structures by means of guided ultrasonic waves, *Journal of Intelligent Material Systems and Structures*, 21 (2010) 1397-1407.

- [30] P. Rajagopal, M. Drozd, E.A. Skelton, M.J. Lowe, R.V. Craster, On the use of absorbing layers to simulate the propagation of elastic waves in unbounded isotropic media using commercially available finite element packages, *NDT & E International*, 51 (2012) 30-40.
- [31] J.R. Pettit, A. Walker, P. Cawley, M. Lowe, A stiffness reduction method for efficient absorption of waves at boundaries for use in commercial finite element codes, *Ultrasonics*, 54 (2014) 1868-1879.
- [32] H. Mohseni, C.-T. Ng, Rayleigh wave propagation and scattering characteristics at debondings in fibre-reinforced polymer-retrofitted concrete structures, *Structural Health Monitoring*, 18 (2019) 303-317.
- [33] X. Hu, C.-T. Ng, A. Kotousov, Ultrasonic guided wave field modeling in a one-side water-immersed steel plate, in: *Lecture Notes in Civil Engineering*, 2021, pp. 1131-1140.
- [34] R. Soleimanpour, C.-T. Ng, Scattering analysis of nonlinear Lamb waves at delaminations in composite laminates, *Journal of Vibration and Control*, (2021) 1077546321990145.
- [35] Abaqus, Abaqus 6.13 Analysis User's Guide, Dassault Systems Simulia Corp, Providence, RI, (2013).
- [36] Q. Xie, C. Ni, Z. Shen, Defects Detection and Localization in Underwater Plates Using Laser Laterally Generated Pure Non-Dispersive S0 Mode, *Applied Sciences*, 9 (2019) 459.
- [37] M. Abbas, M. Shafiee, An overview of maintenance management strategies for corroded steel structures in extreme marine environments, *Marine Structures*, 71 (2020) 102718.
- [38] J. Bingham, M. Hinders, Lamb wave characterization of corrosion-thinning in aircraft stringers: Experiment and three-dimensional simulation, *The Journal of the Acoustical Society of America*, 126 (2009) 103-113.
- [39] V.T. Rathod, D. Roy Mahapatra, Ultrasonic Lamb wave based monitoring of corrosion type of damage in plate using a circular array of piezoelectric transducers, *NDT & E International*, 44 (2011) 628-636.
- [40] T. Gao, H. Sun, Y. Hong, X. Qing, Hidden corrosion detection using laser ultrasonic guided waves with multi-frequency local wavenumber estimation, *Ultrasonics*, 108 (2020) 106182.
- [41] X. Hu, C.-T. Ng, A. Kotousov, Damage Detection of Partially Immersed Plates Using Guided Waves, in: *Recent Advances in Structural Health Monitoring Research in Australia*, Nova Science Publishers Inc., 2021.
- [42] A.E. Takiy, C. Kitano, R.T. Higuti, S.C.G. Granja, V.T. Prado, L. Elvira, O. Martínez-Graullera, Ultrasound imaging of immersed plates using high-order Lamb modes at their low attenuation frequency bands, *Mechanical Systems and Signal Processing*, 96 (2017) 321-332.
- [43] S. Sharma, A. Mukherjee, Damage detection in submerged plates using ultrasonic guided waves, *Sadhana*, 39 (2014) 1009-1034.
- [44] S. Sharma, A. Mukherjee, Ultrasonic guided waves for monitoring corrosion in submerged plates, *Structural Control and Health Monitoring*, 22 (2015) 19-35.
- [45] E. Pistone, K. Li, P. Rizzo, Noncontact monitoring of immersed plates by means of laser-induced ultrasounds, *Structural Health Monitoring*, 12 (2013) 549-565.
- [46] Y. Liu, X. Hong, B. Zhang, A novel velocity anisotropy probability imaging method using ultrasonic guided waves for composite plates, *Measurement*, 166 (2020) 108087.
- [47] L. Yu, Z. Tian, L. Zhao, Gas Accumulation Detection in a Water Tank Using Lamb Waves, in: *ASME 2012 Conference on Smart Materials, Adaptive Structures and Intelligent Systems*, 2012, pp. 807-815.

- [48] A. Takiy, S. Granja, R. Higuti, C. Kitano, L. Elvira, O. Martinez-Graullera, F.M. de Espinosa, Theoretical analysis and experimental validation of the scholte wave propagation in immersed plates for the characterization of viscous fluids, in: 2013 IEEE International Ultrasonics Symposium (IUS), Ieee, 2013, pp. 1614-1617.
- [49] F.B. Cegla, P. Cawley, M.J.S. Lowe, Fluid bulk velocity and attenuation measurements in non-Newtonian liquids using a dipstick sensor, *Measurement Science and Technology*, 17 (2005) 264.
- [50] S. Tietze, J. Schlemmer, G. Lindner, Influence of surface acoustic waves induced acoustic streaming on the kinetics of electrochemical reactions, *SPIE*, 2013.